Universiteit Utrecht

Department of Physics
Institute for Marine and Atmospheric research Utrecht
(IMAU)

Multiple equilibria in the Eocene ocean circulation leading to the Eocene-Oligocene transition

Bachelor Thesis

Denise Ruijsch
6142060

Supervisor:

Dr. A.S. von der Heydt
Institute for Marine and Atmospheric Research, Department of Physics, Utrecht University

June 11, 2020

Abstract

The most marked step from a greenhouse world to the current icehouse world is the transition from the Eocene to the Oligocene, 33.7 Ma. It has been suggested that this transition results from a 'cascade' of two coupled tipping elements, namely the ocean overturning circulation and the Antarctic ice sheet coupled via the carbon cycle. A prerequisite for this cascading tipping mechanism is that in the Eocene ocean circulation multiple steady states exist. In this thesis we will explore this latter issue within a newly developed ocean modelling framework Veros. In particular, we will incorporate the Eocene continental geometry into the ocean model and run the model into steady state by forcing it with an idealised forcing from an existing Eocene climate model simulation. Next, we will search for multiple equilibria by temporarily perturbing the freshwater forcing in this setup. We found that Veros is capable of finding a second equilibrium in the present-day geometry. For the Eocene geometry we did find two different ocean circulations, but not a pronounced second equilibrium. We argue that this is probably because the ocean circulation is highly sensitive to small changes in the surface forcing and that the forcing used in this thesis was too idealised. With this result, we did not prove that there exists a cascading tipping mechanism, but for a next research a less idealised forcing could be used to find multiple equilibria in the Eocene geometry.

Contents

1 Introduction

The climate has changed drastically over the last 65 million years. It went from a warm and basically ice-free world to a world with large ice sheets in both polar regions. This long transition has not been smooth though. There were periods of gradual warming or cooling and periods of rapid climate change (Baatsen et al., 2018) [1]. The most marked step from a greenhouse world to the current icehouse world is the transition from the Eocene to the Oligocene, 33.7 Ma. The Eocene climate was much warmer, with polar deep water temperatures up to 10 degrees warmer than today. Antarctica was already in its current position, ice-free and richly vegetated. Global temperatures dropped at the Eocene-Oligocene transition (EOT). This allowed a semi-permanent ice-sheet to form on Antarctica (Tigchelaar et al., 2011) [2].

The marine δ^{18}O concentration gives the most prominent evidence for this relatively rapid cooling. In paleoclimatology, δ^{18}O is a measure of the ratio of stable isotopes oxygen-18 (^{18}O) and oxygen-16 (^{16}O) and can be used with ice cores to determine the temperature from when the ice was formed. This ratio varies depending on the temperature of the surrounding water, as well as other factors such as the salinity, and the volume of water locked up in ice sheets. The δ^{18}O concentration is determined from foraminifera cores from the ocean floor, which are composed of calcium carbonate and are found in many common geological environments. Numerous cores were taken from the ocean floor and they show that the δ^{18}O concentration increased abruptly with 1.2-1.5‰ in the EOT. This shift lasts for roughly 500 kyr and is marked by a remarkable two-step profile. This profile has two steps of 40 kyr with a plateau of 200 kyr in between. The δ^{18}O concentration remained approximately constant at this plateau. The EOT ends with a sustained maximum in δ^{18}O concentration lasting about 400 kyr. After this time the δ^{18}O concentration decreased again (Coxall et al., 2005) [3]. Eventually the δ^{18}O concentration stabilises to a value $\sim$ 1‰ higher than before the EOT (Coxall and Pearson, 2007) [4].

The two-step profile is suggested by paleorecords. The first step has been frequently interpreted in terms of mostly ocean cooling, while the second step is dominated by major land ice growth. In a previous model study (Tigchelaar et al., 2011) the first step was achieved by a transition in the ocean meridional overturning circulation and the second by a transition from an ice free continent to a glaciated one.

There is evidence that deep water formation was more pronounced in the Southern Ocean than in the Northern Ocean during the Eocene. Sedimentary and seismic evidence in combination with analysis of neodymium (Nd) isotopes shows that there was a transition from a southern sinking source to a bipolar source of deep water formation at the beginning of the Oligocene (Thomas et al., 2003) [5].

The opening or closing of gateways is often used as an explanation of major climate shifts observed in proxy data. The most widely discussed mechanism for the EOT is the opening of the Drake Passage between Antarctica and South-America and of the Tasmanian Passage between Antarctica and Australia. This would have facilitated the emergence of the Antarctic Circumpolar Current (ACC). This thermally isolated Antarctica in such a way that a large ice sheet could appear. However, determining the exact time of this opening has proven problematic. This makes it hard to make a direct causal relationship with climate change (Baatsen et al., 2018). There is a second hypothesis for the EOT. Coupled climate models show that is it far more likely that the transition occurred because of a long term decrease in atmospheric pCO_2 (DeConto and Pollard, 2003; Goldner et al., 2014) [6] [7].

Tigchelaar et al. (2011) proposes that there was also a transition between two stable states of the meridional overturning circulation (MOC). In this model study the first increase in the marine benthic δ^{18}O concentration is the result of the MOC transition from a southern-only deep water formation to a bipolar deep water formation. This transition leads to a cooling of the deep ocean and thus an initial increase in marine benthic δ^{18}O. The second step is induced by lowering the atmospheric pCO2 below a critical threshold value, for which Antarctic land ice will rapidly grow, further increasing the marine benthic δ^{18}O concentration. It was found that the shift in MOC can occur spontaneously by random density fluctuations or induced by tectonic changes, i.e. the opening of the Drake Passage and Tasman Gateway. A possible shift from a southern towards a northern overturning circulation would result in significant changes in the global heat distribution and consequently make the Southern Hemisphere climate more susceptible for significant cooling and ice sheet formation on Antarctica.

It has also been suggested that the EOT results from a 'cascade' of two coupled tipping elements, namely the ocean meridional overturning circulation (MOC) and the Antarctic ice sheet coupled via the carbon cycle. A prerequisite for this cascading tipping mechanism is that in the Eocene ocean circulation multiple steady states exist (Baatsen et al., 2018).

In this thesis we will explore this latter issue within a newly developed ocean modelling framework Veros. First we discuss the theoretical aspect of the MOC, the mathematical framework for multiple steady states in the MOC and the Eocene climate. After that, we will use Veros to try to find a second equilibrium in the present-day configuration. We do this because we first want to know if Veros is capable of finding multiple equilibria with known data. We start by running the present-day model into a steady state. Next, we will search for multiple equilibria by temporarily perturbing the freshwater forcing in this setup. Then, we will restart the model again with the original forcing to see if the model stays in the second equilibrium. Once we find a second equilibrium in the present-day, we will incorporate the Eocene continental geometry into the ocean model and run the model into steady state by forcing it with an idealised forcing from an existing Eocene climate model simulation. Next, we will again search for multiple equilibria by temporarily perturbing the freshwater forcing in this setup and restarting it with the original forcing. If we find a second equilibrium in the Eocene geometry, we can prove that there was a cascading tipping mechanism in the Eocene ocean circulation.

2 Theory

2.1 The Meridional Overturning Circulation (MOC)

One of the most important components in the climate system is the ocean circulation. There are two main driving forces for the ocean circulation, which are both at the surface. Together they drive the tree-dimensional circulation of the ocean. The first driving force is the wind. The wind accounts mostly for the horizontal circulation. The second driving force is driven by the fluxes of heat and fresh water. This accounts mostly for the meridional overturning circulation (MOC). The MOC is defined as the zonally-integrated mass transport in the ocean. It transports large amounts of water, heat and salt around the globe (Drijfhout, S.S. & W. Hazeleger, 2007)[10]. The MOC transports about a fourth of the total heat transport of the ocean. Measurements show that all the deep water is turned over every 600 years (Robert Toggweiler & Caitlin M Amos, 2019)[8].

There are only a few key locations where the density of the water is large enough for it to sink. These sites are mostly at high latitudes because the density of seawater is strongly dependent on temperature. Colder seawater is denser than warmer water. The density of the seawater depends also on its salt content. This means that deep water is formed in the North Atlantic because the water is saltier there. The North Pacific is fresher and that is why deep water does not form there (Schmittner, Chiang & Hemming, 2007)[9].

The most vigorous overturning circulation today is that of the Atlantic Ocean. The upper part of the Atlantic MOC (AMOC) carries the warm water of the upper ocean through the tropics towards the north. The deep part carries cold dense polar water southward around the tip of Africa and into the Southern Ocean beyond. The AMOC converts roughly $15 \cdot 10^6$ m^3s^{-1} of upper water into deep water. Oceanographers use the unit of Sverdrup (Sv), which is defined as 10^6 m^3s^{-1}. That means that the AMOC converts about 15 Sv. All the rivers of the world combined deliver about 1 Sv of freshwater into the ocean. That shows how powerful the AMOC is (Robert Toggweiler & Caitlin M Amos, 2019)[8]. The release of heat from the ocean to the atmosphere in the subpolar North Atlantic makes a major contribution to the relatively mild climate in northwest Europe, which is up to 6 °C warmer than similar maritime climates bordering the Pacific (Weijer, W., Cheng, W., Drijfhout, S. S., Federov, A.V., Hu, A., Jackson, L. C., et al. (2019))[11].

When the MOC moves northward through the tropics, it becomes saltier due to the evaporation of the ocean water. It also becomes warmer and saltier by mixing with the salty outflow from the Mediterranean Sea. At higher latitudes, the ocean cools. Cold water is denser than warm water and that makes polar surface water denser compared to warmer waters at lower latitudes. The final stages of this process make the salty North Atlantic water cold and dense enough to sink, which means that cooling contributes to a stronger MOC. It now appears that most of the deep water sinking in the North Atlantic upwells back to the surface in the Southern Ocean.

The cycling of freshwater between the ocean and the atmosphere (hydrological cycle) results in a net addition of freshwater to the polar region, which reduces the density of the polar surface waters. This means that the salinity-driven part is almost always in opposition to the temperature-driven part. The hydrological cycle is expected to become stronger in the future with global warming. If the hydrological cycle is fairly strong, the freshwater added in high latitudes can create a low-salinity lid that can reduce or annihilate the MOC (Robert Toggweiler and Caitlin M Amos, 2019)[8].

Without temperature-effects, the MOC would reverse, with sinking in the tropics and rising in the subpolar regions. So when the temperature-driven part dominates, the result is a strong MOC characterized by northern sinking. When the salinity-driven part dominates, a much weaker MOC with sinking in the tropics occurs. There is also a regime where they are both of comparable strength. In this regime both states are possible. That means that the MOC is bi-stable. The actual state depends on the history of the MOC. If it was already dominated by the temperature-driven part, it will stay that way if the forcing conditions do not change. The same holds for the salinity driven state. This behaviour is called hysteresis. A perturbation can induce an abrupt transition from one state to another within a few decades. The most conceivable perturbation is a freshwater flux in the North Atlantic. This can be done by, for example, glacier or ice-cap melting. This will always tend to bring the MOC from the temperature-driven state to the salinity-driven state. At this state, the MOC is strongly reduced in strength or even reversed (Drijfhout, S.S. & W. Hazeleger, 2007) [10]. An AMOC collapse would have global consequences and could lead to reduction in surface air temperatures of up to 10 °C in the North Atlantic (Weijer, W., Cheng, W., Drijfhout, S. S., Federov, A.V., Hu, A., Jackson, L. C., et al. (2019))[11].

2.2 Multiple overturning equilibria

The present-day MOC is mainly temperature driven, which means that we have a strong MOC characterised by sinking in the north. It is, in principle, also possible that the evaporation excess in the sub-tropics produces surface water with a very high salinity. That means that the density is higher and that deepwater formation can take place at low latitudes. This water then flows poleward where it can enter an equatorward cold return branch via upwelling (Aken, 2007) [13]. This notion was studied by Stommel (1961) [14] using a density driven two-box model. He showed that two different states of the MOC are possible on a single hemisphere. There can be sinking in the polar box or sinking in the equatorial box. There is also a three-box model developed by Rooth in 1982. This is an interhemispheric model which can be used to explain why there is sinking in the northern Atlantic Ocean in the present day and not in the southern Atlantic Ocean.

2.2.1 Two-Box model

Stommel (1961) devised a single-hemispheric model. He made this model to explore the existence of stable responses to a constant atmospheric forcing with either a temperate-driven or a salinity-driven MOC. The model consists of two boxes, as can be seen in figure 2.1. These boxes are well mixed. One box is at a high latitude (polar box) and the other one is at a low latitude (equatorial box). The polar box is characterized by a low temperature T_1 and salinity S_1, while the equatorial box is characterized by high T_2 and S_2. The boxes are connected with two ducts. One duct represents the near-surface branch of the MOC, and the other one represents the abyssal flow. The abyssal flow is the flow between 3 and 6 kilometers deep. The poleward flow through the near-surface duct amounts to Ψ. This is also equal to the equatorward volume flux in the abyssal duct. The polar box loses a total heat of Q to the atmosphere and receives a net amount of fresh water from precipitation minus evaporation. This is equivalent to a positive virtual salt flux F_S. The boundary conditions ensure that $T_1 < T_2$ and $S_1 < S_2$. Zero atmospheric storage is assumed in the model. That means that there is conservation of heat and fresh water, which means that the heat and virtual salinity exchanges with the atmosphere in both boxes have the same magnitude but opposite signs [13].

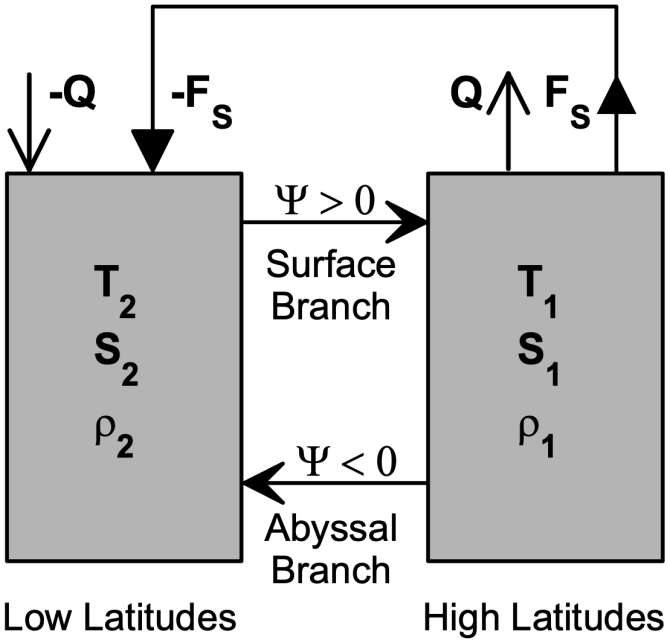

Figure 2.1: A single-hemispheric box model of the MOC. It has two well-mixed boxes, following the scheme introduced by Stommel (1961). The left box represents the low latitudes of the ocean and the right box the high latitudes. If the abyssal branch transports water from the high to the low latitudes, its volume transport Ψ is defined as positive. The total heat flux Q and the virtual salinity flux F_s have the same magnitude but opposite sign at the high and low latitudes because of conservation of heat and salt (Van Aken 2007, p. 243) [13].

The possible solutions of the model will be determined by the prescription of the dynamics of the two-box system, the boundary conditions and the equation of state. Stommel (1961) assumed the surface level in both boxes to be nearly equal. The abyssal density gradient is determined by the density difference between the two boxes. That condition is described by

$$\Psi = \frac{k}{\rho_0}(\rho_1 - \rho_2) \tag{2.1}$$

with k a dimensional linear friction coefficient and ρ_0 a reference density. The surface branch has no dynamics of its own. It follows the overturning circulation because of conservation of mass. If Ψ is positive, the near-surface flow is a warm return flow. This is the situation in the north of the Atlantic ocean in the present-day. When Ψ is negative, relatively saline water with high density can form at low latitudes. This water is then transported to high latitudes by the abyssal branch. With a linear equation of state equation (2.1) becomes

$$\Psi = k\left[\alpha(T_2 - T_1) - \beta(S_2 - S_1)\right] \tag{2.2}$$

with α the the thermal expansion coefficient and β the haline contraction coefficient. According to equation (2.2), if both salinities and temperatures are described as boundary conditions, a single stationary

solution results. Stommel (1961) applied restoring boundary conditions for both Q and F_S, where he took the slower adaptation to the atmospheric forcing of the salinity compared to temperature into account [13]. He did this because if they adapt at the same rate the circulation always advects lighter water into the sinking box, and the sum of the advective feedbacks is always negative. In that case, the model has only one equilibrium. However, when thermal anomalies are removed more quickly than salinity anomalies, then the positive salt-advection feedback can overcome the negative temperature advection feedback. This would result in an additional densification of the subpolar box and a strengthening of the flow (Weijer, W., Cheng, W., Drijfhout, S. S., Federov, A.V., Hu, A., Jackson, L. C., et al. (2019)) [11]. The boundary conditions, however, prevent the system from being solved analytically. Therefore, Marotzke (1990) [15] proposed a simplified set of boundary conditions, which are in principle even more physical than restoring boundary conditions. In order to simulate the relatively fast response of the temperature to the atmospheric forcing in both boxes, he prescribed the temperatures T_1 and T_2 as $T_2 > T_1$. This removes the necessity to formulate a separate conservation equation for both boxes. He prescribed constant virtual salinity fluxes F_S and $-F_S$ for the boxes. That modeled the slower response of the salinity field to atmospheric forcing. We also assume that the flow Ψ brings water with the salinity from the box of origin to the other box [13]. With a unit volume for both boxes the salinity equations become

$$\frac{dS_1}{dt} = -F_S + |\Psi|(S_2 - S_1), \tag{2.3a}$$

$$\frac{dS_2}{dt} = F_S - |\Psi|(S_2 - S_1). \tag{2.3b}$$

It can be seen that the sum of equations (2.3a) and (2.3b) is equal to zero. This indicates that the mean salinity is fixed in time. The equation can be simplified by introducing $\Delta T = T_2 - T_1 > 0$ and $\Delta S = S_2 - S_1 > 0$. The evolution of the salinity difference ΔS can be described subtracting equation (2.3a) from equation (2.3b). That gives

$$\frac{d\Delta S}{dt} = 2F_S - 2|\Psi|\Delta S. \tag{2.4}$$

It is the first term in this equation that leads to the generation of a salinity difference between the boxes. This is damped due the the second term. This is a restoring term due to the MOC [13]. Filling in equation (2.2) into equation (2.4) gives

$$\frac{d\Delta S}{dt} = 2F_S - 2k|\alpha\Delta T - \beta\Delta S|\Delta S. \tag{2.5}$$

This is a nonlinear equation and allows in principle multiple stationary solutions. These solutions can be derived by setting the left hand side of equation (2.5) to zero. Because of the absolute value in this equation, we have to discriminate between a positive and a negative case. We will first look at the positive case. That means that $\alpha\Delta T > \beta\Delta S$, so $\Psi > 0$. In that case the stationary solution is described by: $F_S - k(\alpha\Delta T - \beta\Delta S)\Delta S = 0$. This can be rewritten into

$$(\beta\Delta S)^2 - (\alpha\Delta T)(\beta\Delta S) + \beta F_S/k = 0. \tag{2.6}$$

This is a quadratic equation and has two roots. They are defined as $\beta\Delta S_1$ and $\beta\Delta S_2$ and they are given by

$$(\beta\Delta S)_{1,2} = (\alpha\Delta T)\left[\frac{1}{2} \pm \sqrt{\frac{1}{4} - \frac{\beta F_S}{k(\alpha\Delta T)^2}}\right]. \tag{2.7}$$

For the root to be real, $\frac{\beta F_S}{k(\alpha\Delta T)^2}$ has to be smaller than $1/4$ and that means that the square root is always less than $1/2$. If that condition is fulfilled, the two roots represent two possible stationary MOC circulations for a single forcing. The overturning rate of the MOC is expressed by Ψ. The bigger (+) branch implies a large salinity difference between box 2 and box 1. Then the salinity difference compensates the density difference due to the difference in temperature for a large part. This means that the Ψ will be small. The (-) branch results in a larger density gradient and therefore in a stronger MOC. If the salinity forcing βF_S is bigger than $k(\alpha\Delta T)^2/4$, no real solution is possible. That means that no stationary thermally driven MOC can exist.

If $\beta\Delta S > \alpha\Delta T$, so $\Psi < 0$, then the MOC is driven by the salinity excess in the low-latitude box. Equation (2.5) can then be written as $F_S + k(\alpha\Delta T - \beta\Delta S)\Delta S = 0$. This can be rewritten as

$$(\beta\Delta S)^2 - (\alpha\Delta T)(\beta\Delta S) - \beta F_S/k = 0. \tag{2.8}$$

This has two roots, which are defined as

$$(\beta\Delta S)_{3,4} = (\alpha\Delta T)\left[\frac{1}{2} \pm \sqrt{\frac{1}{4} + \frac{\beta F_S}{k(\alpha\Delta T)^2}}\right]. \tag{2.9}$$

The root $(\beta\Delta S)_4$ is not a solution for this problem, because that gives a negative value, and that contradicts our assumption that $\beta\Delta S > \alpha\Delta T$.

Next, we have to write the stationary solutions as dimensionless salinity gradients to make the equations more comprehensible. We define $G^* = \beta\Delta S/\alpha\Delta T$. This is a function of the dimensionless forcing $F^* = \beta F_S/k(\alpha\Delta T)^2$. Then the dimensionless overturning rate is $\Psi^* = \Psi/k\alpha\Delta T = (1 - G^*)$ [13]. From the solutions (2.7) and (2.9) for G^* we then get the dimensionless solutions for Ψ^*

$$\Psi^*_{1,2} = (1 - G^*_{1,2}) = \frac{1}{2} \mp \sqrt{\frac{1}{4} - F^*}, \tag{2.10a}$$

$$\Psi^*_3 = (1 - G^*_3) = \frac{1}{2} - \sqrt{\frac{1}{4} + F^*}. \tag{2.10b}$$

Ψ^* will be equal to 1 without any salinity forcing. We now introduce a dimensionless time unit, defined as $t^* = 2k\alpha\Delta T t$ [13]. Equation (2.5) can then be written as

$$\frac{dG^*}{dt^*} = F^* - |1 - G^*|G^*. \tag{2.11}$$

This results in an equation for the derivative of Ψ^*:

$$\frac{d\Psi^*}{dt^*} = -F^* + |\Psi^*|(1 - \Psi^*). \tag{2.12}$$

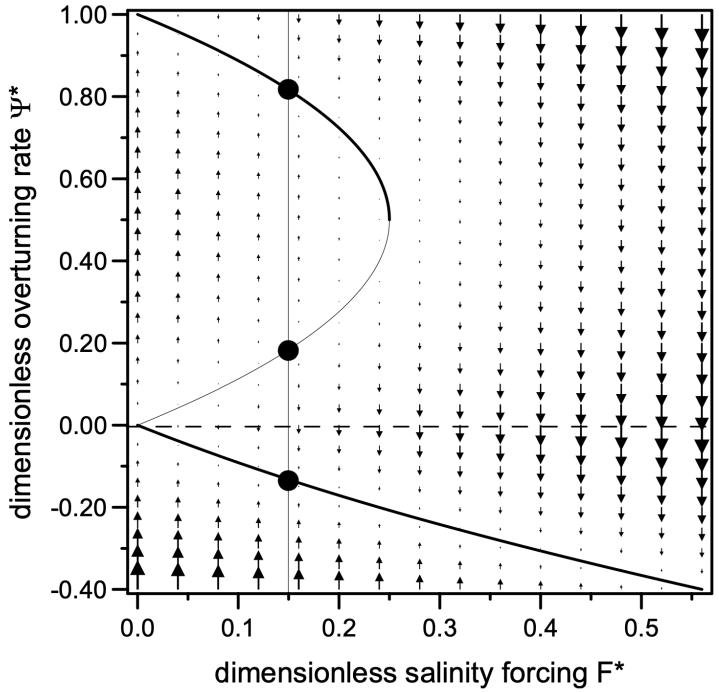

Figure 2.2: The solutions of equations (2.10a) and (2.10b). Here the dimensionless overturning rate Ψ^* is plotted against the dimensionless salinity forcing F^*. The full line shows the possible stationary solutions. The black dots are the three possible dimensionless salinity gradients Ψ^* for a F^* smaller than $1/4$. The arrows represent $\frac{d\Psi^*}{dt^*}$ given by equation (2.12) (Van Aken 2007, p. 247) [13].

Figure 2.2 represents the dimensionless forcing and the overturning. The stationary solutions are represented by a full line. Solutions with $\Psi^* > 0$ represent the thermally-driven MOC according to equation (2.10a). This means that there is sinking in the polar box. Solutions with $\Psi^* < 0$ represent the salinity-driven MOC according to equation (2.10b), with sinking in the equatorial box. The full line with $\Psi^* > 0$ is divided into two parts. The thick line corresponds to a fast thermally driven circulation. This has a low salinity contrast between the boxes. The thin line corresponds with the slow thermally driven mode. This has a large salinity difference between the boxes. It appears that for a dimensionless salinity forcing F^*, smaller than $1/4$, three possible stationary responses Ψ^* exist, shown by the black dots in figure 2.2. It can be seen that the time derivative is very small close to the stationary solutions. For $F^* < 1/4$ and for initial positions between the zero F^* line and the parabola, $\frac{d\Psi^*}{dt^*}$ is directed to the upper thick line. For initial positions with $F^* > 1/4$ the solution is attracted towards the negative, salinity-driven stationary solution. For initial conditions on the thin line, $\frac{d\Psi^*}{dt^*}$ is away from that branch. That means that this stationary solution is unstable and will never be reached. It can be seen that it depends on the position of the initial conditions which stationary state will be reached.

If the circulation in Stommel's two-box model of the MOC is in the fast thermally driven circulation (upper thick line, figure 2.2) and the salinity forcing F^* increases, the response will follow the thick line closely. It will follow this line until $F^* = 1/4$ and $\Psi^* = 1/2$. There is no thermally driven stationary

solution for a larger forcing. That means that $\frac{d\Psi^*}{dt^*}$ will force the solution to the salinity-drive circulation (lower thick line, figure 2.2). These points are called a saddle point bifurcation and this type of behaviour is typical for back-to-back saddle node bifurcations. To return the circulation to the thermally driven mode, it is not enough to bring F^* back to a value below $1/4$. That is because the salinity-driven stationary mode is stable there. Only if F^* is reduced to zero can the thermally driven mode be reached again [13]. A sketch of the two different solutions in the two-box model is given in figure 2.3.

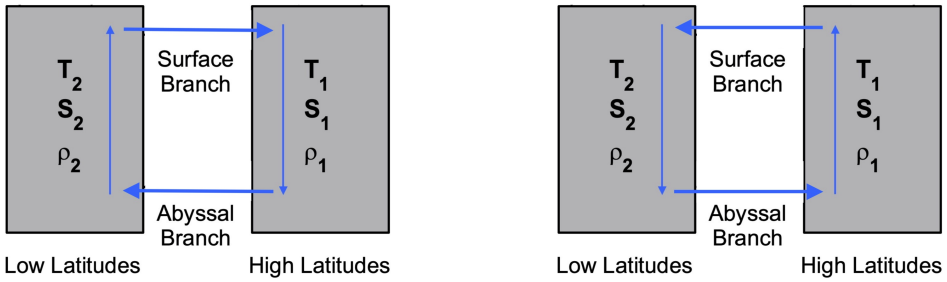

(a) The thermally driven MOC with sinking in the polar box.

(b) The haline driven MOC with sinking in the equatorial box.

Figure 2.3: The two possible states of the MOC, according to Stommel (1961). The blue arrows represent the movement of the MOC.

There are multiple ways to make the model go from the positive overturning rate to the negative overturning rate. Rahmstorf (1996)[12] applied a perturbation in surface forcing. This way its amplitude is increased very slowly, so that the MOC is assumed to remain close to the actual equilibrium for a given forcing state. For some value of the forcing perturbation amplitude, the MOC starts to collapse, marking its transition to the collapsed equilibrium state. When that equilibrium has been reached, the forcing perturbation is typically reduced in strength, until the MOC starts to spin-up again (Weijer, W., Cheng, W., Drijfhout, S. S., Federov, A.V., Hu, A., Jackson, L. C., et al. (2019)) [11].
In this thesis we will use a approach referred to as "hosing", shown in figure 2.4. Here, an instantaneous surface forcing perturbation is applied. This moves the system to the stable branch of the negative Ψ^*. Next, the perturbation is removed. This puts the system back into the bi-stable regime of F^*.

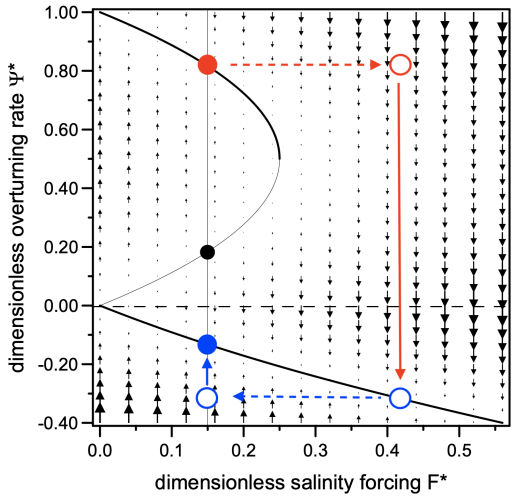

Figure 2.4: Schematic representation of the procedure of the classical hosing experiment. Here, an instantaneous surface forcing perturbation is applied. The red lines indicate the instantaneous perturbation. The blue lines indicate the removed perturbation.

2.2.2 Three-Box model

Stommel's two-box model offers a fundamental explanation of multiple steady states in a single-hemisphere MOC. Its applicability in simulating the behavior of the global MOC, or even the Atlantic MOC, is however limited. It does not contain a cold branch from the cold northern North Atlantic to the even colder Southern Ocean or from the Southern Ocean to the North Pacific Ocean. In order to study the MOC on a global scale, Rooth (1982) [16] developed a tree-box model. This is an interhemispheric model, and can be seen in figure 2.5.

The boxes is this model are also assumed to be well-mixed. In the present day, the northern downwelling box of this model is located at the Arctic Sea. The southern upwelling box begins south of the tip of Africa, approximately 35° South. Here it is introduced into the circumpolar current [13]. The volume of the downwelling box in the north is taken as unit volume. The equatorial box has a volume V_E and the southern downwelling box has a volume V_S. While Rooth (1982) mainly focused on the stability with symmetric salinity and temperature forcing, his model was further elaborated by Scott et al. (1999) [17]. He allowed asymmetric forcing of the temperature and salinity field.

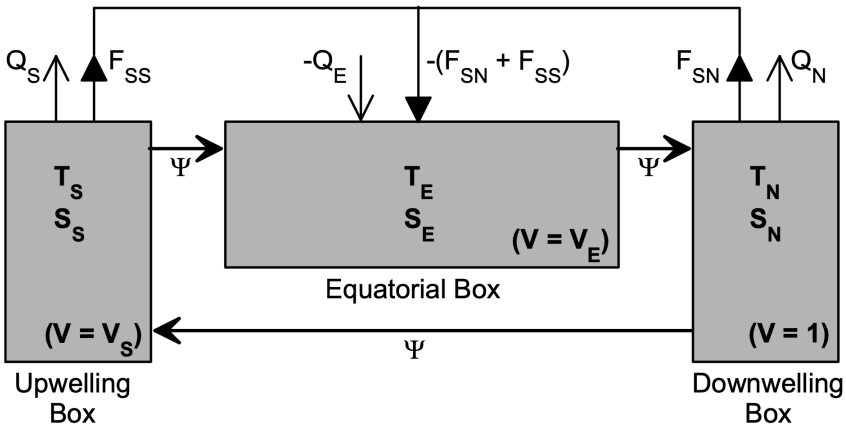

Figure 2.5: A scheme following Rooth's interhemispheric box model. There are two polar boxes and one equatorial box. The polar boxes have volume 1 and volume V_S. There is surface cooling (Q_N and $Q_S > 0$) and an upward virtual salt flux (F_{SN} and F_{SS}) due to a precipitation excess. The polar boxes maintain a relatively low salinity and temperature. The equatorial box has a volume V_E. This box is warmed by air-sea interaction ($Q_E < 0$). The equatorial salinity is increased by a virtual mass flux, equal to $-(F_S N + F_S S)$. This is due to a net evaporation excess and conservation of salt. The deep branch of the MOC transports water between both polar boxes with an overturning rate Ψ (Van Aken 2007, p. 249) [13].

The MOC of this model has a transport rate of Ψ between the boxes. The present day Atlantic MOC (AMOC) is drawn in figure 2.5, with the abyssal Ψ drawn from north to south. However, it is also possible that there is a situation where the circulation direction is contrary to the present day AMOC, with $\Psi < 0$. Similar to the dynamic equation used in the two-box Stommel model, there is a dynamic equation that relates the abyssal Ψ to the density difference between the two polar boxes. With the use of a linear equation of state the dynamics are described by

$$\Psi = k[\alpha(T_S - T_N) - \beta(S_S - S_N)]. \tag{2.13}$$

The value of k will be different than in the two-box model. That is because the typical density differences between the two polar boxes are much smaller than the pole to equator density contrast. The shallow return flow has no dynamics of its own but is governed by volume conservation. The equations that describe the development of the temperature in each box in the present day MOC ($\Psi > 0$) are (Scott et al. 1999) [17]:

$$\frac{dT_N}{dt} = -Q_N + \Psi(T_E - T_N), \tag{2.14a}$$

$$\frac{dT_E}{dt} = -\frac{Q_E}{V_E} + \frac{\Psi(T_S - T_E)}{V_E}, \tag{2.14b}$$

$$\frac{dT_S}{dt} = -\frac{Q_S}{V_S} + \frac{\Psi(T_N - T_S)}{V_S}. \tag{2.14c}$$

Q_N and Q_S are the integrated heat losses to the atmosphere of both polar boxes. They are both greater than zero. $-Q_E$ is the heat gain in the cross-equatorial box ($Q_E < 0$).

The total salt content is conserved. That means that while changes in the box volumes due to evaporation and precipitation are ignored, the sum of the virtual salinity restoring flux F_S for the three boxes will be zero. For each box, F_S is determined by a combination of evaporation, precipitation and river runoff into that box. F_S is approximated by $F_S = -S_0(E - P + R)$. Here, S_0 is the reference salinity. The net amount of water in the ocean does not change. This results in the following equations for the salinity of the boxes [13]:

$$\frac{dS_N}{dt} = -F_{SN} + \Psi(S_E - S_N), \tag{2.15a}$$

$$\frac{dS_E}{dt} = \frac{(F_{SN} - F_{SS})}{V_E} + \frac{\Psi(S_S - S_E)}{V_E}, \tag{2.15b}$$

$$\frac{dS_S}{dt} = -\frac{F_{SS}}{V_S} + \frac{\Psi(S_N - S_S)}{V_S}, \tag{2.15c}$$

With F_{SN} the virtual salinity flux for the northern polar box and F_{SS} the virtual salinity flux for the southern polar box. They are both greater than zero.
Stationary solutions of equations (2.14) and (2.15) have zero time derivatives. These solutions are indicated with an overbar. Next, we substitute the stationary form of equations (2.14c) and (2.15c) into equation (2.13). That results in an equation for the stationary overturning $\overline{\Psi}$:

$$\overline{\Psi}^2 = k(-\alpha Q_S + \beta F_{SS}). \tag{2.16}$$

This implies that the stationary overturning rate $\overline{\Psi}$ is proportional to the square root of the net virtual mass flux due to air-sea interaction over the upwelling box only.
According to equation (2.14c), equation (2.16) can also be written as:

$$\overline{\Psi} = k\left[-\alpha(\overline{T}_N - \overline{T}_S) + \beta\frac{F_{SS}}{\overline{\Psi}}\right]. \tag{2.17}$$

This quadratic equation of the stationary overturning rate $\overline{\Psi}$ has as solution (Rahmstorf 1996) [12]:

$$\overline{\Psi} = -\frac{\alpha k(\overline{T}_N - \overline{T}_S)}{2} \pm \frac{1}{2}\sqrt{k^2\alpha^2(\overline{T}_N - \overline{T}_S)^2 + 4k\beta F_{SS}}, \tag{2.18}$$

which depends on the virtual salinity flux over the upwelling box, and the temperature difference between both polar boxes. The variable F_{SS} in equation (2.18) is $F_{SS} = (F_{SS} + F_{SN}) - F_{SN} = -F_{SE} - F_{SN}$, with F_{SE} the virtual salinity flux of the equatorial box [13].
Changes is F_{SN} and F_{SE} can affect the response of the model. An increase of F_{SN} will dilute the water in the northern downwelling box. This leads to a reduction of $\overline{\Psi}$. The model will then adjust the salinities in the boxes until the original F_{SS} governed stationary equilibrium transport is reached again. When there is, for example, a massive freshwater influx from a melting Greenland ice cap, a transition to a new equilibrium solution with inverted overturning direction may be triggered [13].

So far we have only discussed the MOC with a positive overturning rate Ψ, but it is also possible for the MOC to have a negative overturning rate ($\Psi < 0$). Here, the same solution structure as discussed so far exists, but downwelling will be found in the southern Polar box and upwelling in the northern Polar box. To derive the six appropriate temperature and salinity equations similar to equations (2.14) and (2.15) only the advective terms have to be adapted. This is due to the equatorial symmetry of the model. The solutions for a positive and negative overturning $\overline{\Psi}$ allow two stationary circulations with

pole-to-pole flow in either direction, and thus cross-equatorial flow and heat transport [13]. The total bifurcation behaviour can be seen in figure 2.6. The bifurcation diagram presented in figure 2.6 shows a considerable increased level of complexity for the three-box model relative to the two- box model. In the diagram, β is used as a control parameter and represents the dimensionless freshwater flux. $\Theta_n - \Theta_s$ is proportional to the temperature difference between the northern en southern Polar boxes (Dijkstra, 2005) [18].

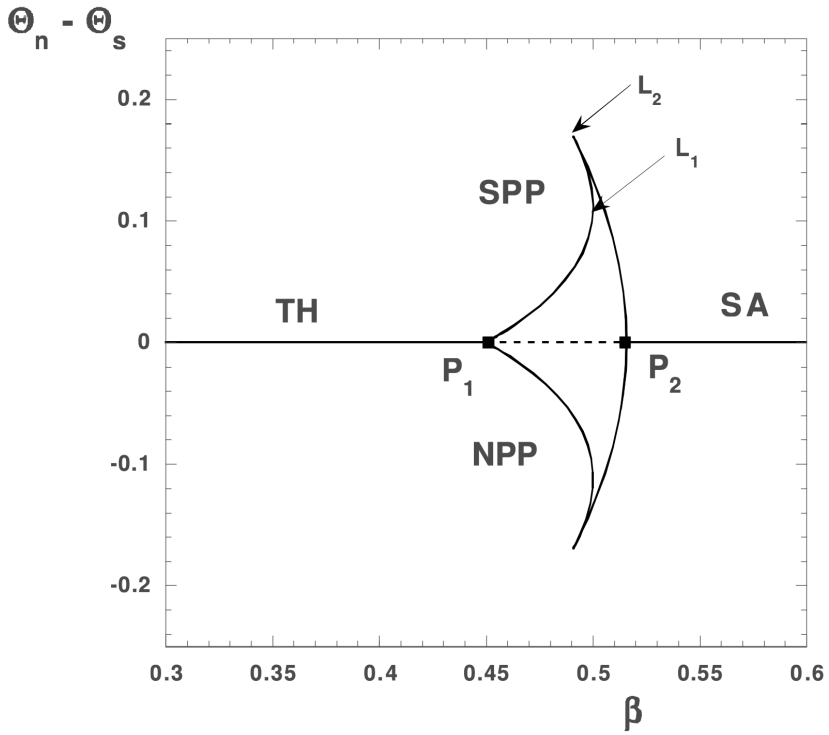

Figure 2.6: Bifurcation diagram of the three-box ocean model with a symmetric surface forcing. $\Theta_n - \Theta_s$ is zero when the solutions are symmetric with respect to the equator (Dijkstra 2005, p. 73) [18].

The drawn line indicates stable steady solutions and the dashed line indicates unstable steady solutions. The short branch between L_1 and L_2 contains unstable solutions. For a small freshwater forcing, there is only one symmetric solution with upwelling at the equator and sinking at the poles (TH). At P_1, the TH solution becomes unstable and the equatorial symmetry is broken. Two asymmetric solutions appear under symmetric forcing conditions. These solutions are sinking in the North and upwelling in the South (NPP) and sinking in the South and upwelling in the North (SPP). For these solutions, there is no longer equatorial upwelling, but only upwelling at one of the poles. For larger freshwater forcings, only the SA solution exists with downwelling at the equator. It is apparent that the NPP and SPP states exist besides each other, for the same freshwater forcing [18]. Sketches for all these solutions are shown in figure 2.7. In this situation there is only a fast transition possible from an SPP to an NPP state, but more options are present when the freshwater forcing is asymmetric. The bifurcation diagram splits into two detached branches, consequently allowing for fast transitions between all combinations of asymmetric (NPP, SPP) and symmetric (TH, SA) overturning circulations (Dijkstra & Weijer, 2003) [19].

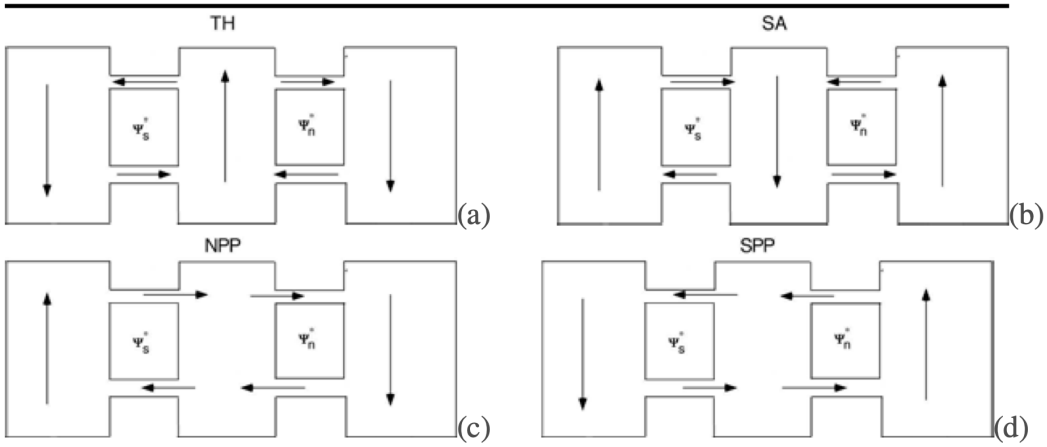

Figure 2.7: Sketch of the four different solutions within the three-box model. a) TH solution. b) SA solution. c) NPP solution. d) SPP solution. [18]

Results of these simple box models (e.g. the opposing effect of the thermal and haline equator-to-pole differences and the occurrence of multiple steady states) help understand the dynamics of the MOC in the real ocean better (Olbers, Dirk & Zhang, Jian. (2008)) [20]. It is, however, still an open question of how well such simple box models represent reality. They only represent the world to a limited extend. The two- and three-box models both consider a single ocean, but researchers have proposed models that consider a coupled system of different oceans, for example the Atlantic Ocean and the Pacific Ocean (Jian Zhang (2007)) [21]. The stability of the AMOC in the present-day can be estimated from real world observations. Previous studies suggest that the AMOC is likely bi-stable in the present-day. This estimation is however very sensitive to the choice of observational data (Liu, Wei & Liu, Zhengyu. (2013)) [22].

2.3 The Eocene Climate

The Eocene is a geological epoch that lasted from 56 to 33.9 Ma. It contained a wide variety of different climate conditions that includes the warmest climate in the Cenozoic Era. The Eocene ends in an icehouse climate, during which the first semi-permanent ice sheets formed on Antarctica. In the Eocene period, continents were arranged much as they are today but they were bunched more closely together. The Atlantic Ocean was much smaller than it is today. During the Eocene, the continents continued to drift toward their current positions (Stanley and Luczaj, 2015) [23].

The transition between the Paleocene and Eocene epochs (56 Ma) was marked by a sudden global warming. This warming has been linked to volcanism, causing extreme changes in Earth's carbon cycle and a significant temperature rise (Gutjahr et al., (2017)) [24]. The total volume of glacial ice on earth was quite small at the time. The climate warmed to what is know as the Early Eocene climate optimum. During that time, the temperature gradients between the equator and the poles were relatively gentle. Greenhouse warming was stronger during the Early Eocene than it is today and forests were much more widespread [23].

During the beginning of the Middle Eocene (49 Ma), climates at high latitudes cooled significantly. The carbon dioxide concentration started decreasing due to to increased siliceous plankton productivity and marine carbon burial (Pearson, P. N.; Palmer, M. R. (2000)) [25]. The climate kept cooling into the Late Eocene (38 Ma). Figure 2.8 shows estimates of the Cenozoic temperature changes in the deep sea. It can be seen that after the Early Eocene climate optimum, the temperature dropped in the Middle and Late Eocene. Since global cooling began, forests have never been as widespread on Earth as they were before [23].

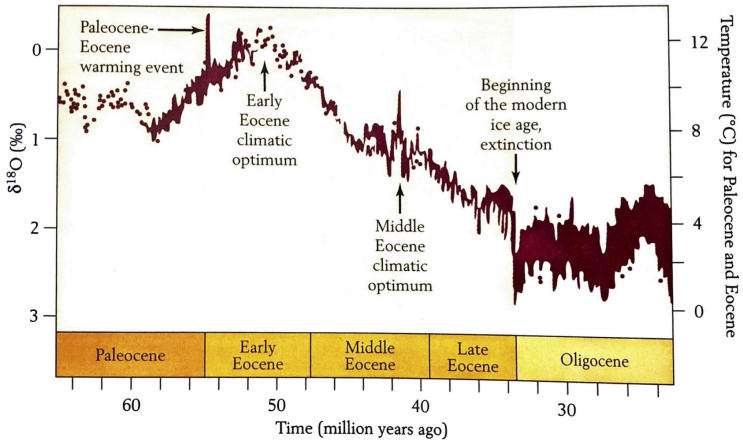

Figure 2.8: Estimates of the Cenozoic temperature changes in the deep sea based on oxygen isotope ratios in deep-sea foraminifera (Stanley and Luczaj, 2015, page 462) [23].

At approximately 34 Ma, another major climate transition occurred, which is known as the Eocene-Oligocene transition (EOT). The EOT marks the shift from the so-called "greenhouse world" to the "icehouse world", during which the first semi-permanent ice sheets formed on Antarctica. The cause of the transition is however not well understood, particularly the role of ocean circulation. The prevailing proposed mechanisms for the transition are a decline in atmospheric CO2 below a critical threshold and the opening of Southern Ocean gateways causing the thermal isolation of Antarctica (Hutchinson et al., 2018) [26]. During the EOT, Australia and South America drifted away from Antarctica. That left Antarctica isolated in a Polar position. This allowed the Antarctic Circumpolar Current (ACC) to emerge during the EOT. In the middle Eocene, warm currents flowed from the southern oceans to warm Antarctica. When the ACC emerged, these waters got trapped in a current around Antarctica, where they became very cold [23].

The evolution of the MOC around the EOT remains a topic of debate. Global compilations of benthic foraminiferal stable isotopes of δ^{13}C and δ^{18}O suggest that there was a high latitude Southern Hemisphere deep water formation. Nd isotope distributions also suggest that vigorous bipolar sinking in the Pacific Ocean, with dominating deep water formation in the southern Pacific Ocean [26]. Deep water formation is in the Southern Ocean is favored by the closed Drake and Tasmanian passages. The strong MOC sustains the poleward advection of saline subtropical water to the Southern Ocean, maintaining deep water formation. This salt-advection feedback mechanism works similarly in the present-day North Atlantic overturning circulation (Zhang et al., (2020)) [27].

3 Model description

3.1 General Layout of Veros

For over 50 years, numerical simulations have been used to advance our understanding of the ocean circulation. Especially for regimes that are difficult to treat analytically, they have become irreplaceable. Computing resources available have been massively increased over the last 20 years. This leads to a shift from process studies to analysis of climate model output. There are however still basic questions about ocean dynamics that remain unanswered. That is why Veros (the Versatile Ocean Simulator) was built in 2018 [28]. Veros is the first global-scale ocean simulator in pure Python. Their main goal is an open source ocean code that is easy to access, easy to use, easy to verify and easy to modify. Veros is an adaptation of pyOM2 (v2.1.0), developed by Carsten Eden (Institut für Meereskunde, Hamburg University) [30]. It solves the full three-dimensional primitive equations (hydrostatic equations) in three dimensions.

The ocean interior is mostly adiabatic and has a long memory, easily exceeding 1000 years (e.g., Gebbie and Huybers, 2006) [29]. That way, experiments can take several months to complete because this requires long integration times for numerical models. Programming languages like Python are usually designed with the explicit goal of improving code structure and thus readability [28].

The model used in this thesis is a four-degree model, which means that every grid cell is 4 degrees in longitude and 4 degrees in latitude. The model runs from 78° North to 78° South, which gives a total of 90 grid cells in the x-direction and 40 grid cells in the y-direction. The model gives 4 output files every model year: the averages, the overturning, the energies and a snapshot. These files are constantly updated while the model runs. At the end of the whole run, a restart file is written. The model can be restarted with this file. For this thesis, the averages and overturning files will be the most used ones. In the averages file the surface salinity flux, the sea surface salinity (SSS) and the sea surface temperature (SST) is found. In the overturning file we find the 'vsf depth'. This is the meridional transport. To add a perturbation, the output file of the surface salinity flux can be adapted. This file is then used as a temporary forcing for a restart of the model.

The restoring salinity flux defined in the model is:

$$\text{Surface salinity flux} = \frac{1}{t_{\text{rest}}} \cdot (SSS - \text{salinity}(z = -35\text{m})).$$

Here, SSS is the sea-surface salinity in g/kg. This value does not change. The SSS in this formula is the salinity data from the present-day that is read into the model from external files. The model then calculates the difference between the initial and measured salinity and divides this by the restoring time (t_{rest}). In this model, the restoring time is a month. When there is a difference in salinity, a salinity flux emerges. This flux transports the salt from areas with a high salinity to areas with a low salinity.

The surface heat flux defined in the model is:

$$\text{Surface heat flux} = \text{Q}_{\text{net}} + \text{Q}_{\text{nec}} \cdot ((SST - \text{temperature}(z = -35\text{m}))/(c_{p_0} \cdot \rho_0)).$$

Here, SST is the sea-surface temperature. Q_{net} is the net heat flux and Q_{nec} is the necessary heat flux in W/m^2. These heat fluxes fluctuate for every month. c_{p_0} is the specific heat capacity in $\text{J}/(\text{kg} \cdot \text{K})$ and ρ_0 is the surface density in m^3/kg. When there is a difference in temperature, a heat flux emerges. This flux

transports the heat from areas with a high temperature to areas with a low temperature and is defined in $K \cdot m/s$.

3.2 Model for the present-day

Veros has a section in the code where it reads input data from external files. For the present-day model, these files will be used. First, the model needs to go to an equilibrium with these forcings. This is reached when the MOC becomes constant. We will look at a depth of 1080 m and at 20° North, which is where the northern sinking of MOC can be observed in the present-day. This point is often close to the maximum meridional overturning stream function in models. There is also an array of measurement devices across the North Atlantic at approximately 26° North. An equilibrium is tried to be reached by running the model for 1000 years. A time series of the MOC is shown below. The blue line represents the meridional transport in Sv.

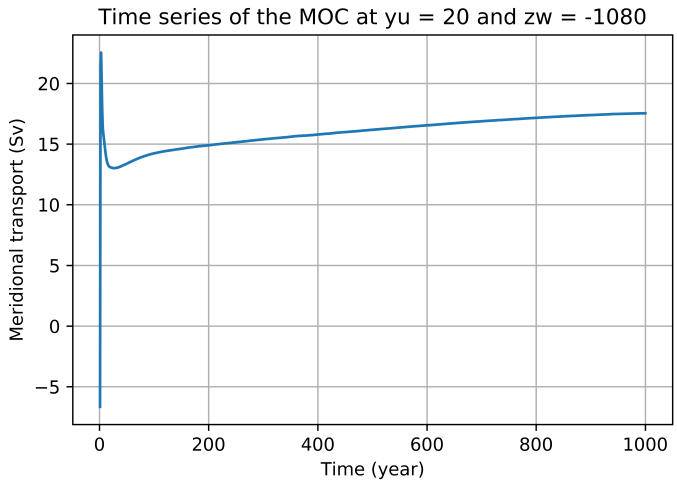

Figure 3.1: A time-series of the meridional transport for 1000 years at a depth of 1080 m and 20° North. The blue line indicates the meridional transport in Sv.

It can be seen in figure 3.1 that the overturning starts of very irregular. It then becomes more constant as the time progresses. After 1000 years, it has become as good as constant. We can now look at the latitude-vertical contour plot of year 1000. In this plot, the depth is plotted against the latitude. The blue values represent a negative overturning, and the red values a positive overturning. It can be seen in figure 3.2 that we have currently a northern sinking. This can be seen due to the fact that positive values of the MOC moving in a clockwise direction. When there is a southern sinking, the output would look different. The transport in the North would be much weaker, or even negative. That way the MOC would move anti-clockwise and there would be sinking in the south.
The ACC can also be seen in the south. The vertical coordinate starts at 500 meters depth, because the wind dominates in the upper 500 meters. The red cell in the south is known as the Deacon Cell.

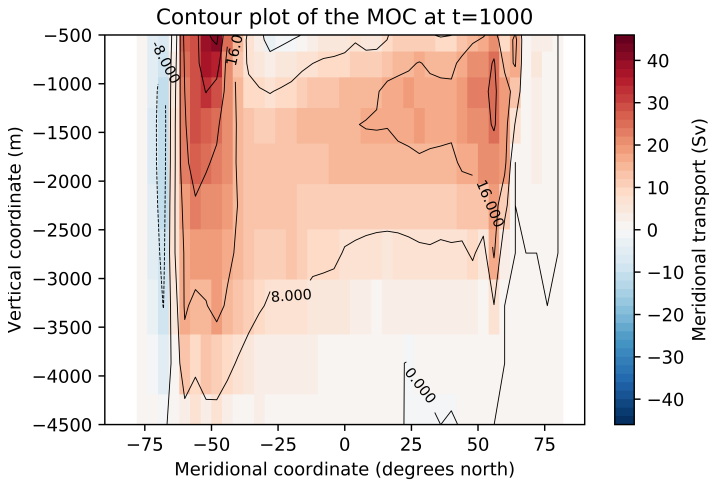

Figure 3.2: A latitude-vertical contour plot of the overturning at year 1000. The red values represent a positive (clockwise) overturning and the blue values a negative (anti-clockwise) overturning.

Next, we take the output file of the surface salinity flux of year 1000 and use this as a new surface salinity flux, instead of the restoring salinity flux defined in the model. To do this, the output file with the averages has to be read into Veros. From this file, the surface salinity flux can be read, which can then be prescribed as a new surface salinity flux. We let this run for another 20 year to make sure we are in equilibrium and stay that way.

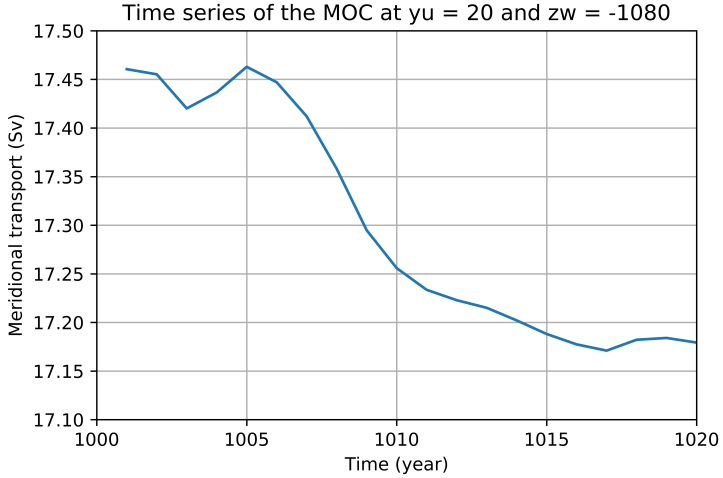

Figure 3.3: A time-series of the meridional transport for 20 years at a depth of 1080 m and 20° North, under a prescribed surface salinity flux, starting from year 1000. The blue line indicates the meridional transport in Sv.

It can be seen in figure 3.3 that the overturning becomes weaker, but the changes are minimal. In figure 3.4, the latitude-vertical contour plot of year 1020 is shown. It can be seen that this looks very much like figure 3.2.

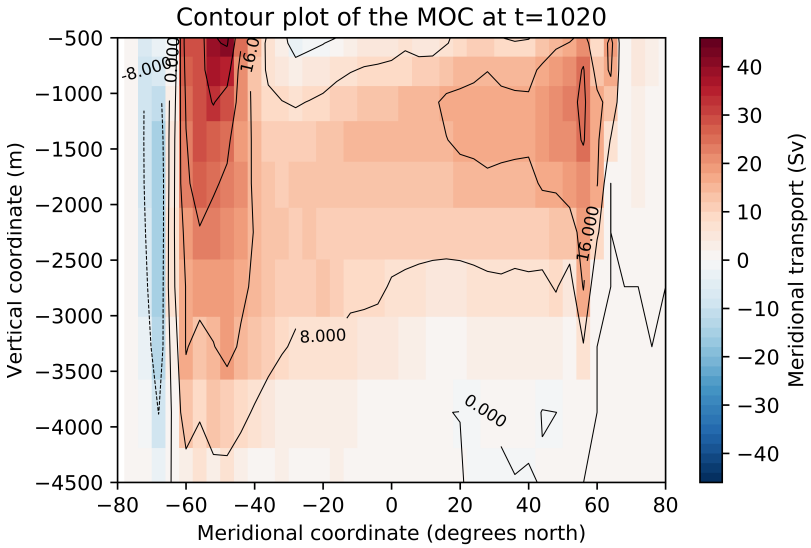

Figure 3.4: A latitude-vertical contour plot of the overturning at year 1020. The red values represent a positive (clockwise) overturning and the blue values a negative (anti-clockwise) overturning.

Because the changes are minimal, we can now add a perturbation to find the second equilibrium. Similarly to Baatsen et al. (2018) [31], we add a perturbation of 1 Sv. But instead of adding it to the Northern Pacific for the Eocene geometry, we add it to the Northern Atlantic for the present-day. This is because the Atlantic MOC is the most vigorous overturning circulation in the present-day.
We add a freshwater flux of 1 Sv in the northern Atlantic (50° to 70° North and 306° to 350° East) to find the second equilibrium. To keep the total salt content conserved, the sum of all the surface salinity fluxes still has to be zero. This means that 1 Sv of fresh water also has to be subtracted from the ocean.

In the model we however have a surface salinity flux as input instead of a freshwater flux. An addition of fresh water is equal to a subtraction of salt water, which means that we have to subtract 1 Sv from the northern Atlantic Ocean to add the perturbation in Veros.
First we divide 1 Sv over the northern Atlantic Ocean. The unit of the surface salinity forcing (F) in the output file is $(\mathrm{m} \cdot \mathrm{g})/(\mathrm{kg} \cdot \mathrm{s})$. This means that the corresponding subtracted salt water in Sv should be $F \cdot A$, with A the total area in m^2. This leads to $F \cdot A = 1$ Sv. To calculate the numeric value of the surface salinity forcing, both F and A have to be written out in their units. That gives: $F = f \cdot (\mathrm{m} \cdot \mathrm{g})/(\mathrm{kg} \cdot \mathrm{s})$, where f is the numeric value and $(\mathrm{m} \cdot \mathrm{g})/(\mathrm{kg} \cdot \mathrm{s})$ are the units and $A = a \cdot \mathrm{m}^2$, with a the numeric value and m^2 the unit. We then fill this in:

$$
\begin{aligned}
F \cdot A &= 1 \text{ Sv} \\
f \cdot (\text{m} \cdot \text{g})/(\text{kg} \cdot \text{s}) \cdot a \cdot \text{m}^2 &= 1 \text{ Sv} \\
f \cdot 10^{-3}\text{m/s} \cdot a \cdot \text{m}^2 &= 10^6 \text{m}^3/\text{s} \\
f \cdot a &= 10^9
\end{aligned}
$$

The total ocean area (a) in Veros is $6.24866374 \cdot 10^{12}$ m^2. That gives $f = 1.6 \cdot 10^{-4}$. Now we have to give each grid cell a part of the forcing f that corresponds to their size. So each grid cell should get $f_n = f \cdot a_n/a$, where a_n is the size of a single grid cell. This gives a value for the surface salinity flux at each grid cell that has to subtracted from the original flux at that grid cell.

The same can be done for the whole ocean. That gives a surface salinity flux value for each grid cell that has to be added. These new values are added to a new file, which can be added to Veros. This new file with the perturbation is then read into the model instead of the surface salinity flux of year 1000. The surface salinity flux of the perturbed state can be seen in figure 3.5b. Figure 3.5c shows the difference between the surface salinity flux of year 1020 and the file with the perturbation added. It can be seen that the values in the North Atlantic are changed, and that the values for the rest of the world stay nearly the same.

This procedure can be related to the two-box model of Stommel. In the box model we would never find the second equilibrium if we prescribed a fixed salinity in any of the boxes. But when we allow the freshwater to go in and out of the boxes, we can.
As described in section 2, the sea surface thermal forcing acts opposite to the haline forcing from the freshwater flux. The strong negative feedback between the SST and the surface heat flux removes changes in the sea surface temperature rapidly. The difference in the boundary conditions for temperature and salinity may give rise to multiple equilibria of the thermohaline circulation under identical boundary conditions. Therefore, the thermohaline circulation can switch from one equilibrium to another rapidly if the thermal or haline forcing is perturbed (Park, Young-Gyu (1999))[32].
The same thing happens in Veros. In these 3D ocean models we call the combination of a restoring SST and a prescribed freshwater flux mixed boundary conditions. The idea behind it is that an atmosphere would not react to salinity changes in the ocean, while for the SST it does. These mixed boundary conditions are considered a bit more realistic if you have to do it with an ocean-only model.

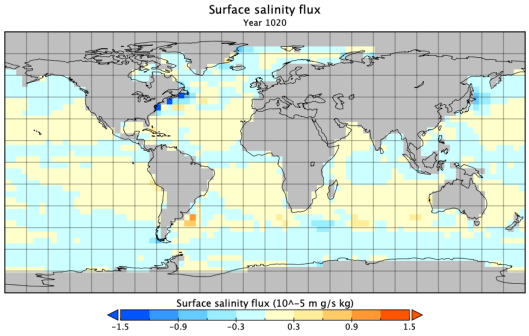

(a) The surface salinity flux of year 1020

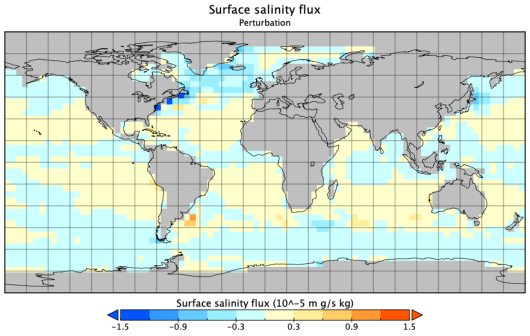

(b) The perturbed surface salinity flux

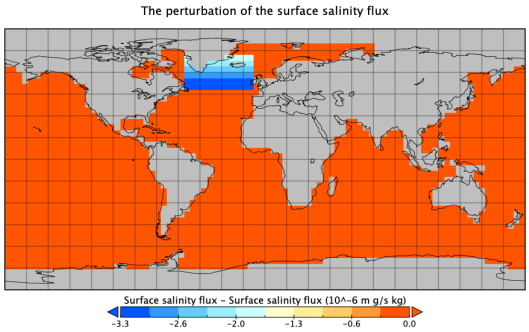

(c) The difference between figures a and b.

Figure 3.5: A longitude-latitude plot of the of the surface salinity flux of year 1020, the perturbation and the difference between them. The blue values represent the subtraction of salinity flux, so an addition of freshwater. In the areas with red values there is a net addition in salinity, so a reduction in freshwater.

When the model is then run for another 60 years with the perturbation (starting from year 1020), it can be seen in figure 3.6 that the meridional transport becomes significantly smaller. This gives a weaker MOC, which can also be seen in figure 3.7. The MOC becomes weaker because the added freshwater makes the Northern Atlantic Ocean less dense, which makes it more difficult for the water to sink.

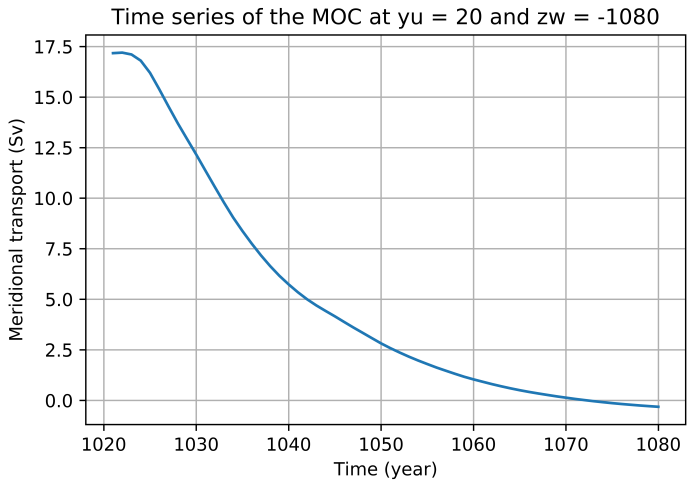

Figure 3.6: A time-series of the meridional transport for 60 years at a depth of 1080 m and 20° North, starting from year 1020. The blue line indicates the meridional transport in Sv.

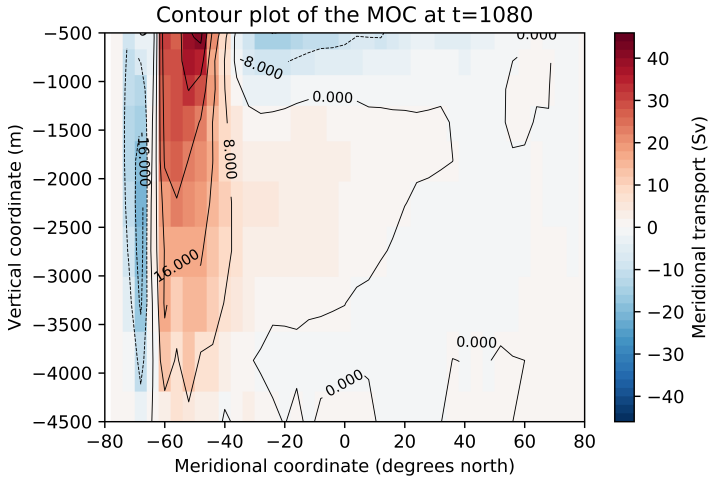

Figure 3.7: A latitude-vertical contour plot of the overturning at year 1080. The red values represent a positive (clockwise) overturning and the blue values a negative (anti-clockwise) overturning.

After the perturbation, the model is run again for 420 year (until year 1500) with the surface salinity forcing from year 1020. The total time series of the MOC can be seen in figure 3.8:

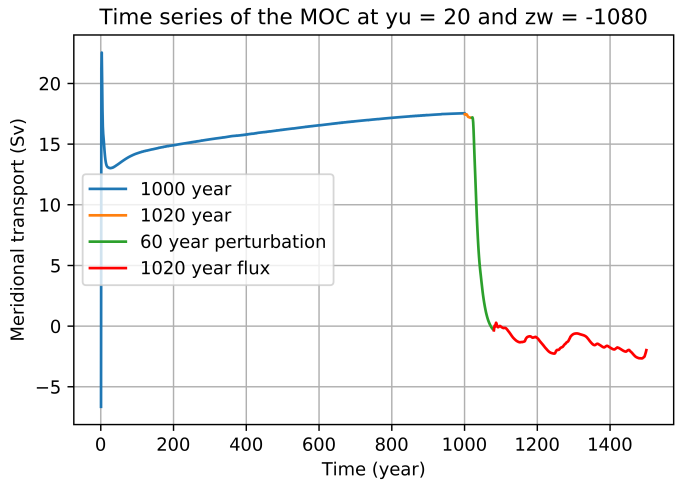

Figure 3.8: The total time-series of the meridional transport for 1500 years at a depth of 1080 m and 20° North. The blue line represents the MOC with the restoring salinity forcing. The yellow line indicates the MOC with the salinity forcing from year 1000. The green line represents the MOC with the perturbation added. The red line represents the MOC with the 1020 year salinity forcing.

It can be seen that the MOC continues to have a negative meridional transport after the perturbation. This means that we have found a new equilibrium. This can also be seen in figure 3.9, which shows that the deep water formation in the North is as good as gone. In some places even an upwelling is visible (blue values).

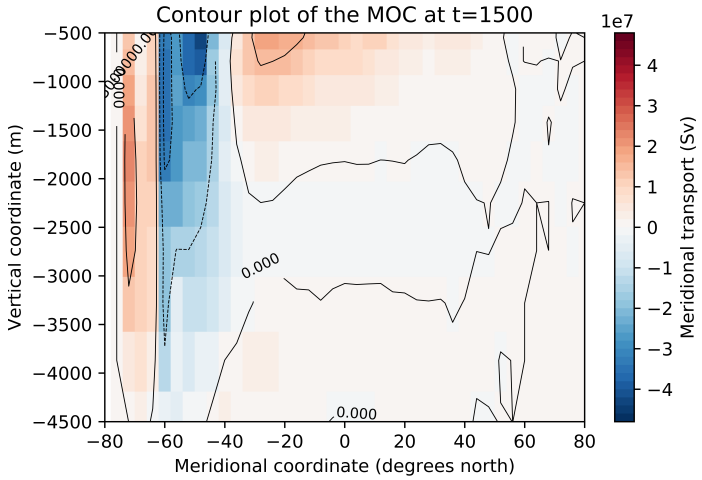

Figure 3.9: A latitude-vertical contour plot of the overturning at year 1500. The red values represent a positive (clockwise) overturning and the blue values a negative (anti-clockwise) overturning.

Figure 3.10 shows that the the SSS in year 1000 is very different than the SSS in year 1500 (420 year after perturbation). The ocean has become much fresher in the North Atlantic Ocean, where the perturbation was added. Figure 3.11 shows that the SST in year 1000 is warmer in the North Atlantic Ocean than in year 1500. These patterns of the SSS and SST appear under exactly the same forcing conditions. The only thing that is different is the MOC, which means that the salinity and temperature distributions change when the MOC changes from deep water formation in the North Atlantic Ocean to deep water formation in the Southern Ocean.

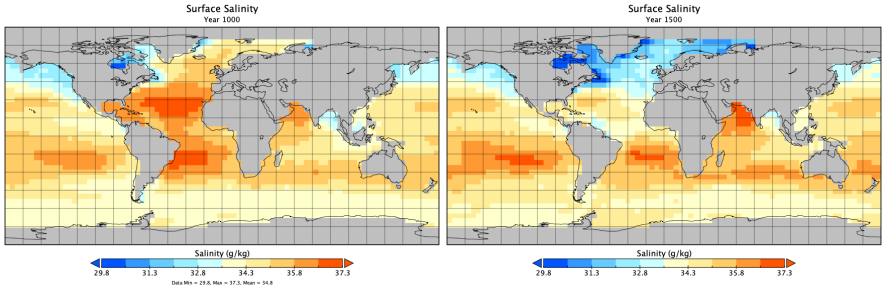

(a) The sea surface salinity of year 1000 (b) The sea surface salinity of year 1500

Figure 3.10: The different sea surface salinities. It can be seen that the ocean has become less salty in the North Atlantic after the perturbation.

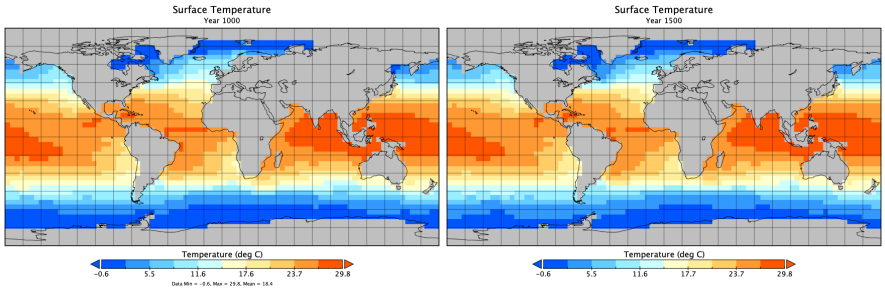

(a) The sea surface temperature of year 1000 (b) The sea surface temperature of year 1500

Figure 3.11: The different sea surface temperatures. It can be seen that the ocean has become colder in the North Atlantic after the perturbation.

3.3 Model for the Eocene geometry

Now that we have found a second equilibrium in the present-day ocean, we can to do the same for the Eocene geometry. Marte Voorneveld did this for his Bachelor thesis, and we will use his setup. He implemented the Eocene geometry of 35 Ma, and made simplified forcing conditions. He made his own forcing conditions because there is no data available for 35 Ma. The used forcing profiles can be seen in section A.1. We note that using idealized forcing conditions will probably induce errors, but we think it will still be possible to find a second equilibrium. The bathymetry used for this setup can be seen in figure 3.12. The most pronounced differences are the closing of the Drake Passage and the opening of the Panama Seaway. It can also be seen that the Tasmanian Passage has become much more shallow.

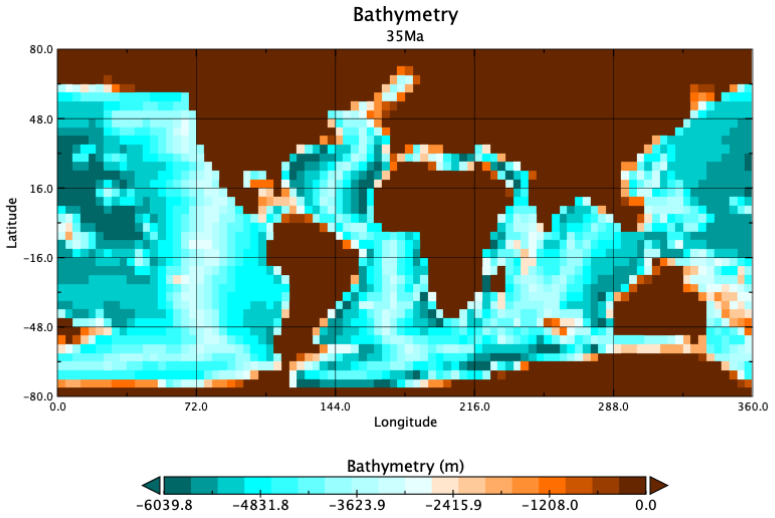

Figure 3.12: The used bathymetry of the Eocene (35 Ma). The dark brown values represent a bathymetry above sea-level.

First, we let the model run for 500 years. The contour plot can be seen in figure 3.13. It can be seen that the values of the meridional transport are much lower than in the present-day setup. Figure 3.14 shows the time-series of the meridional transport for these 500 years.

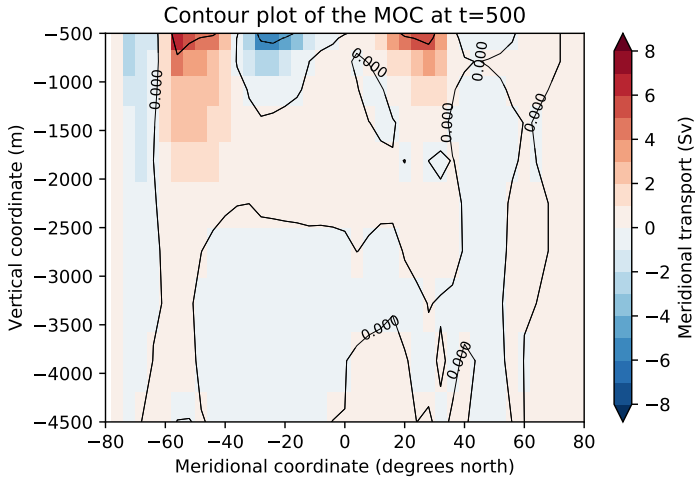

Figure 3.13: A latitude-vertical contour plot of the overturning at year 500. The red values represent a positive (clockwise) overturning and the blue values a negative (anti-clockwise) overturning.

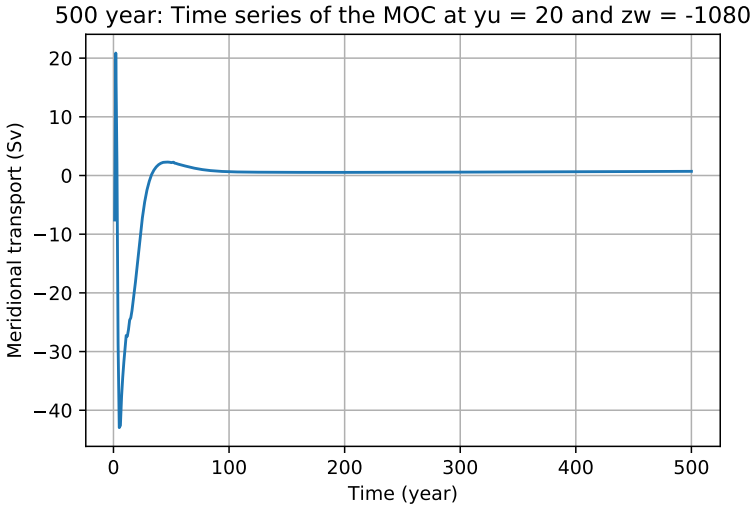

Figure 3.14: A time-series of the meridional transport for 500 years at a depth of 1080 m and 20° North. The blue line indicates the meridional transport in Sv.

Now, we restart the model for another 100 years with the surface salinity flux of year 500, instead of the restoring forcing. The contour plot and time series can be seen in figures 3.15 and 3.16.

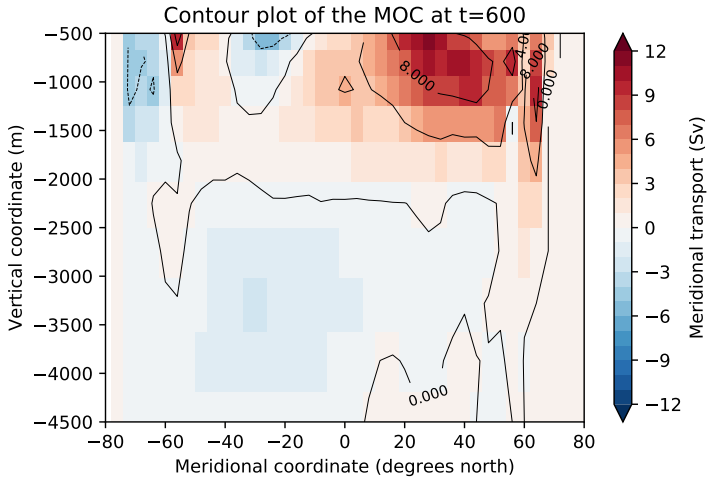

Figure 3.15: A latitude-vertical contour plot of the overturning at year 600. The red values represent a positive (clockwise) overturning and the blue values a negative (anti-clockwise) overturning.

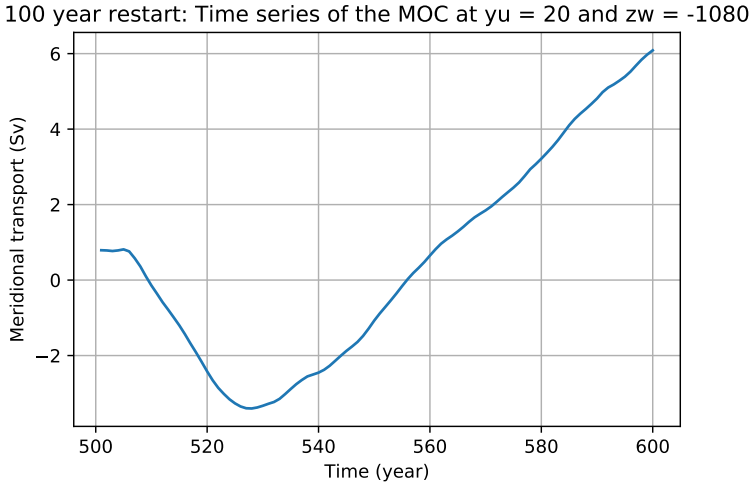

Figure 3.16: A time-series of the meridional transport for 100 years at a depth of 1080 m and 20° North, starting from year 500. The blue line indicates the meridional transport in Sv.

It can be seen in figure 3.16 that the MOC has grown in strength during the 100 year restart, which means that the ocean was not yet in equilibrium at year 500. At year 600, the MOC is still growing in strength. This means that the MOC is also not in equilibrium at year 600. Figure 3.15 shows that we have a more pronounced deep water formation in the north at year 600 than at year 500.

Next, we add a perturbation. To know where to add the perturbation, we have to determine where sinking takes place. This can be done by looking at the longitude-latitude plot of the surface density (figure 3.17).

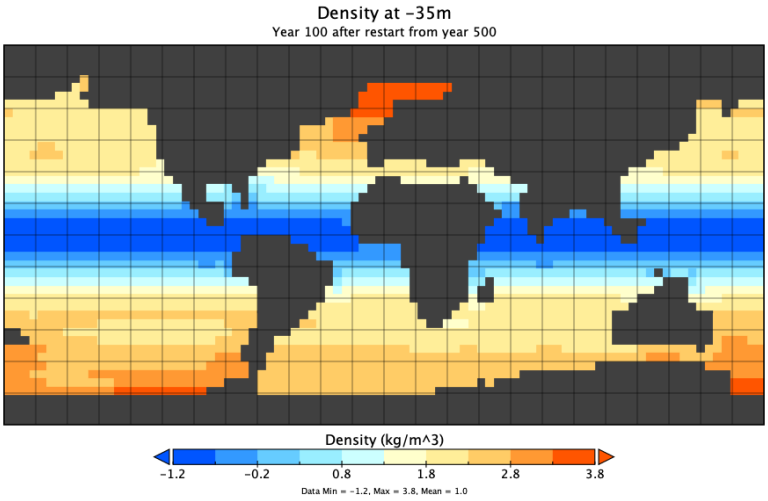

Figure 3.17: A longitude-latitude plot of the surface density at year 600. The highest density can be seen in the Northern Atlantic Ocean, which means that deep water formation takes place there.

Figure 3.17 shows that according to this model sinking takes place in the North Atlantic Ocean, just as in the present day. This means that we can add the perturbation again in the North Atlantic Ocean. The geometry did however change, so the coordinates of the perturbation have to change as well. We chose to add the perturbation between 42°and 70°N and 306°and 30°E. The perturbation is added in the same way as in section 3.2. We again divide 1 Sv of fresh water over the perturbation area, and subtract 1 Sv from the whole ocean. A longitude-latitude plot of the perturbation of the surface salinity flux in shown in figure 3.18. It can be seen that the surface salinity flux changes in the North Atlantic, but stays nearly the same in the rest of the world.

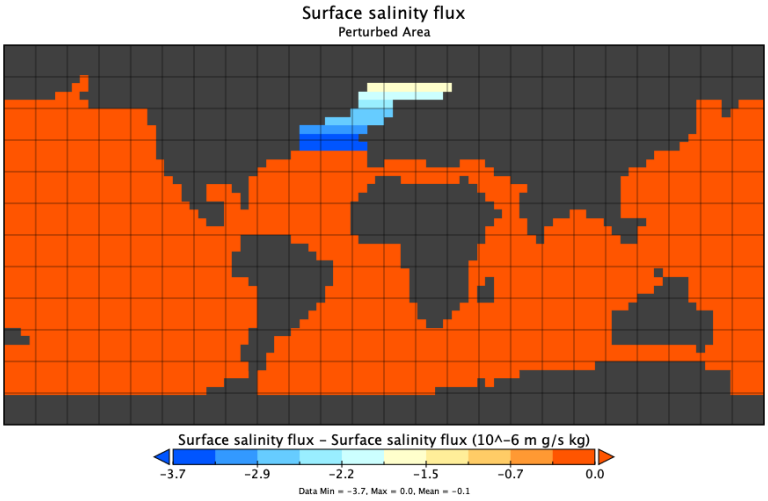

Figure 3.18: A longitude-latitude plot of the perturbation of the surface salinity flux. The blue values represent the subtraction of salinity flux, so an addition of freshwater flux. In the red values there is a net addition in salinity, so a reduction in fresh water.

When we let the model run for another 100 years with perturbation (starting from year 600), it can be seen in figure 3.19 that at first the meridional transport becomes significantly smaller. This gives a weaker MOC. After about 15 years, the meridional transport however becomes stronger again. In the end the MOC is positive again. The latitude-vertical contour plot of the MOC at year 700 can be seen in figure 3.20. It can be seen that the MOC has become weaker, but not much.

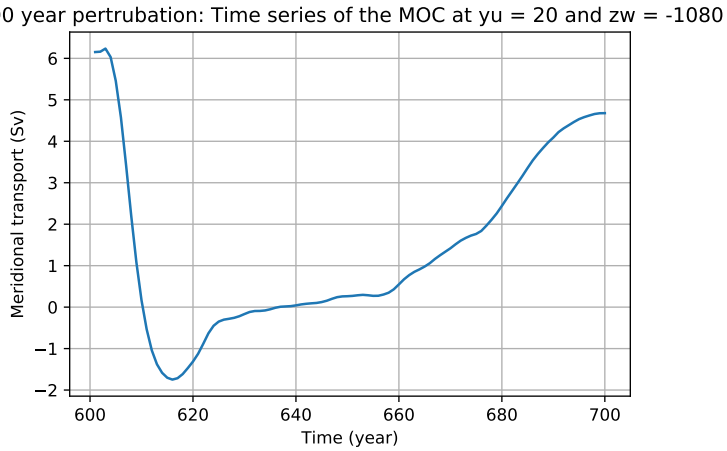

Figure 3.19: A time-series of the meridional transport for 100 years at a depth of 1080 m and 20° North, starting from year 600. The blue line indicates the meridional transport in Sv.

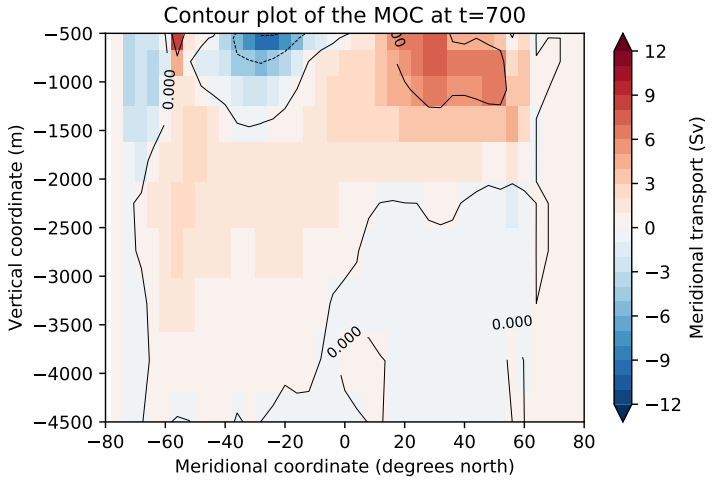

Figure 3.20: A latitude-vertical contour plot of the overturning at year 700. The red values represent a positive (clockwise) overturning and the blue values a negative (anti-clockwise) overturning.

After the perturbation, we let the model run again for 200 years (until year 900) with the surface salinity flux from year 600. In figure 3.21 can be seen that the MOC at first becomes weaker and tends to stay around 0 Sv. However, after year 850 the overturning starts to fluctuate again. Figure 3.22 shows the latitude-vertical contour plot of the overturning at year 900. It can be seen that the clockwise overturning in the North has been reduced and that the counterclockwise overturning in the South has been increased.

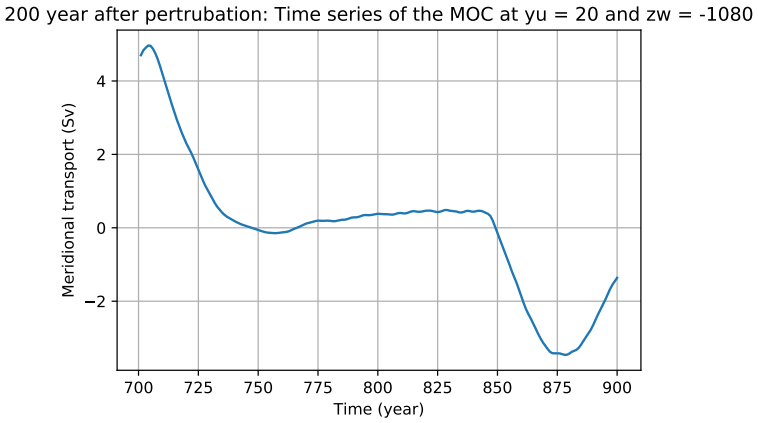

Figure 3.21: A time-series of the meridional transport for 200 years at a depth of 1080 m and 20° North, starting from year 700. The blue line indicates the meridional transport in Sv.

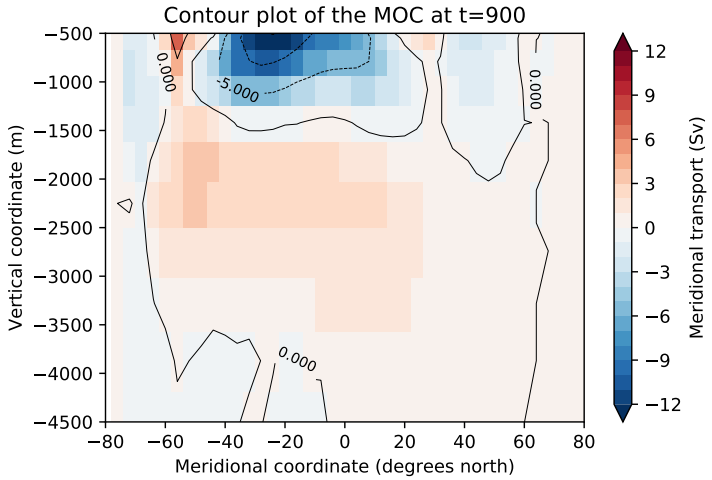

Figure 3.22: A latitude-vertical contour plot of the overturning at year 900. The red values represent a positive (clockwise) overturning and the blue values a negative (anti-clockwise) overturning.

4 Results

The total time series of the MOC at 20 °N and 1080 meters depth in the Eocene geometry can be seen in figure 4.1:

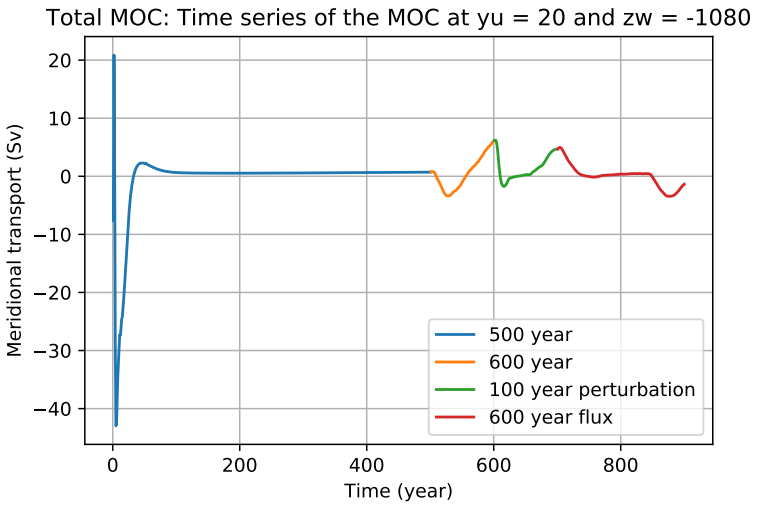

Figure 4.1: The total time-series of the meridional transport for 900 years at a depth of 1080 m and 20° North. The blue represents the MOC with the salinity restoring forcing. The yellow line indicated the MOC with the surface salinity forcing from year 500. The green line represents the perturbation. The red line represents the MOC with the surface salinity flux from year 600.

It can be seen that the meridional transport tends to go to zero. During the 100 year restart with the surface salinity flux from year 500 (yellow line in figure 4.1), the meridional transport does not stay as good as constant constant, as it did in the present-day model. The perturbation (green line) makes the meridional transport negative at first, but after 15 years it becomes positive again. When the model is then restarted with the surface salinity flux from year 600 (red line), the meridional transport goes down again. It seems to stay constant around 0 Sv, but at year 850 it starts to fluctuate again.

Figure 4.2 shows three latitude-vertical contour plots of the overturning at year 500, year 600 and year 900. It can be seen that the overturning changed. At first, the clockwise overturning in the North grows stronger. At year 900, the clockwise overturning in the North and South has decreased, and an anti-clockwise overturning emerged in the South. Especially the differences between figures 4.3b and 4.3c suggest that a second equilibrium could be possible. It can be seen that the overturning is more shallow than in the present-day model. Where the overturning reached a depth of about 3000 meters in the present-day configuration, the overturning reaches about 1000 meters in depth in the Eocene geometry.

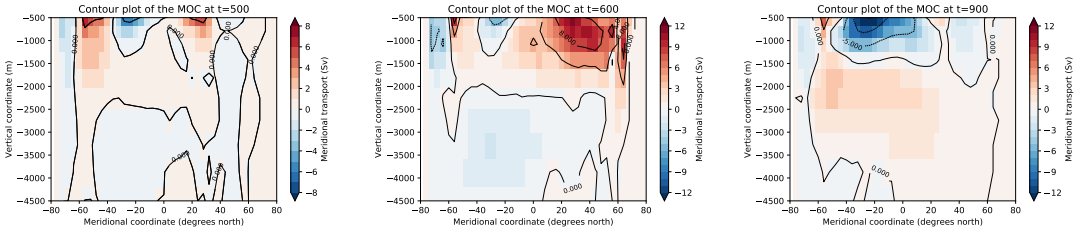

(a) Contour plot of the MOC at year 500.

(b) Contour plot of the MOC at year 600.

(c) Contour plot of the MOC at year 900.

Figure 4.2: Three latitude-vertical contour plots of the overturning at year 500, year 600 and year 900. The red values represent a positive (clockwise) overturning and the blue values a negative (anti-clockwise) overturning.

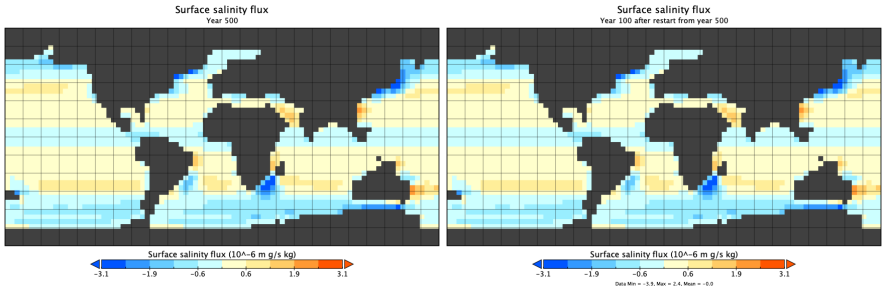

(a) A longitude-latitude plot of the surface salinity flux at year 500.

(b) A longitude-latitude plot of the surface salinity flux at year 600.

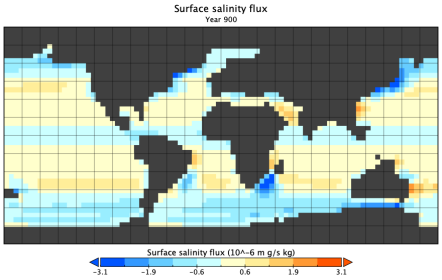

(c) A longitude-latitude plot of the surface salinity flux at year 900.

Figure 4.3: Three longitude-latitude plots of the surface salinity flux at year 500, year 600 and year 900. The red values represent a positive surface salinity flux and the blue values represent a negative surface salinity flux.

Figure 4.3 shows the surface salinity forcing. It can be seen that it stays the same. This is because from year 500 on, we used the prescribed surface salinity flux, instead of the restoring flux defined in the model. Only from year 600 to 700 did we use the perturbed surface salinity flux.

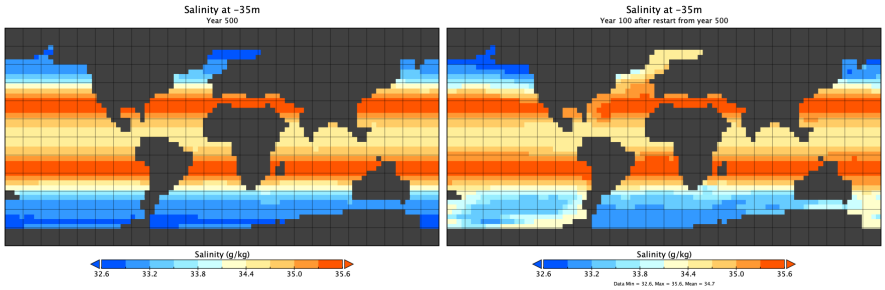

(a) A longitude-latitude plot of the SSS at year 500.

(b) A longitude-latitude plot of the SSS at year 600.

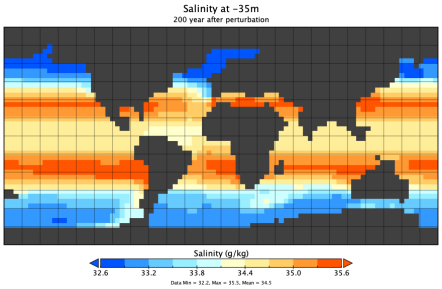

(c) A longitude-latitude plot of the SSS at year 900.

Figure 4.4: Three longitude-latitude plots of the SSS at year 500, year 600 and year 900.

Figure 4.4 shows three longitude-latitude plots of the SSS at year 500, year 600 and year 900. It can be seen that after 500 years the SSS has not changed much from the initial forcing conditions (section A.1). The SSS has changed drastically in year 600, which was when we replaced the restoring surface salinity flux with the constant surface salinity flux of year 500. The North Atlantic Ocean has become much more salty at year 600. The salt from the equator has also spread more over the ocean in year 600. Figure 4.4c shows that the North Atlantic Ocean has become much less salty after we added the perturbation.

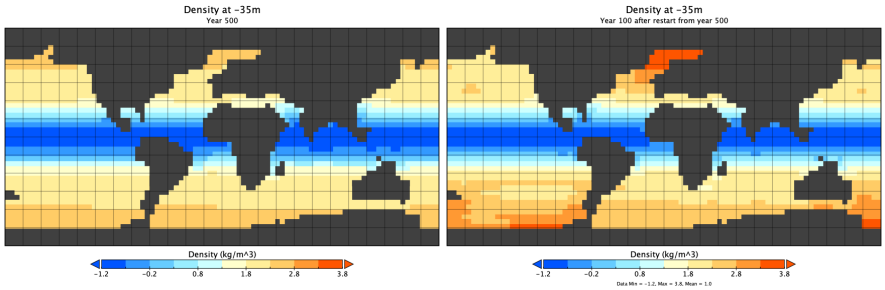

(a) A longitude-latitude plot of the surface density at year 500.

(b) A longitude-latitude plot of the surface density at year 600.

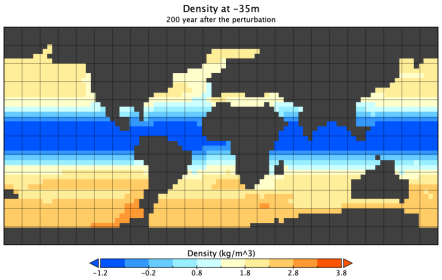

(c) A longitude-latitude plot of the surface density at year 900.

Figure 4.5: Three longitude-latitude plots of the surface density at year 500, year 600 and year 900.

Figure 4.5 shows three longitude-latitude plots of the the density at year 500, year 600 and year 900. From figure 4.5a it is hard to determine where the deep water formation takes place. However, figure 4.5b shows the highest density in the North Atlantic Ocean, which means that deep water formation takes place there in this model. There are also two small regions with a higher density in the southern Pacific Ocean in figure 4.5b. There could also be deep water formation in those regions. From figure 4.5c it is hard to determine where the deep water formation takes place. The density is highest in the southern regions, which means that deep water formation could take place there. It is however not a high density, so there is neither a pronounced southern nor a pronounced northern deep water formation.

Figure 4.6 shows three longitude-latitude plots of the SST at year 500, year 600 and year 900. It can be seen that the SST in figure 4.6a is nearly the same as in figure A.1. The polar regions in figure 4.6b have become slightly warmer. After the perturbation (figure 4.6c), the polar regions have become cooler again.

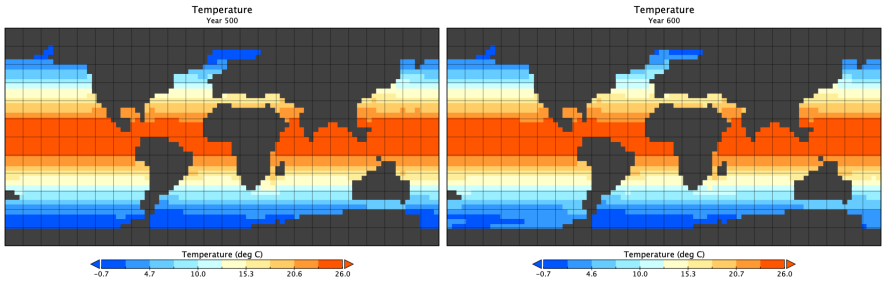

(a) A longitude-latitude plot of the SST at year 500.

(b) A longitude-latitude plot of the SST at year 600.

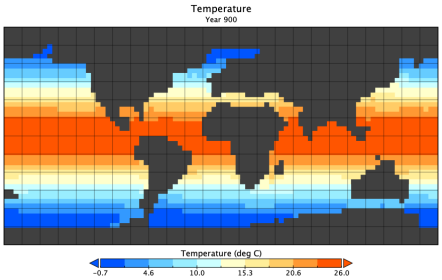

(c) A longitude-latitude plot of the SST at year 900.

Figure 4.6: Three longitude-latitude plots of the SST at year 500, year 600 and year 900.

5 Discussion

5.1 Model for the present-day

Figure 3.8 shows that we have found a constant negative overturning after the perturbation, which means that we have found a second equilibrium in the present-day setup. This is in accordance with studies from for example Marotzke and Willebrand (1991) [33]. Most studies also use a 4° model. Huisman et al. (2010) also find multiple equilibria in the the Atlantic MOC. Dijkstra (2008) [34] finds an initial meridional transport of around 15 Sv for the reference state, which is about the same strength as we found. After the perturbation, Dijkstra (2008) also finds a constant overturning just below 0 Sv. This means that our results are consistent with other studies on multiple equilibria in the present-day MOC.

5.2 Model for the Eocene geometry

As we saw in figure 4.1, the Eocene MOC does not have a constant negative overturning rate after the perturbation, as it did in the Stommel two-box model of section 2.1 and the present-day configuration of section 3.2. Although there is a negative overturning present at year 900, it is still fluctuating and even becoming stronger. The total time series fluctuates around 0 Sv. This means that 20°N and 1080 meters depth was perhaps not the right measure for the Eocene MOC. The yellow line in figure 4.1 should have stayed as good as constant, as in the present-day configuration, because we prescribed a constant surface salinity flux. The fact that it did not stay constant could be because the surface salinity flux was not yet constant after 500 years with the restoring surface salinity flux. Because of this, the perturbation and the red line in figure 4.1 also fluctuated. One way to find out if this is the case is to run the model with the restoring salinity flux until the surface salinity flux is constant in time. Then we need to run it again for 100 years with the surface salinity flux from the last model year and see if it stays constant.

This would however not explain why the Eocene MOC in figure 4.3a is weaker than expected. Baatsen et al. (2020) [36] modeled the Eocene geometry with a fully coupled atmosphere-land-ice-ocean general circulation model and found a contour plot of the MOC. They also found a weaker MOC than in the present-day, but not as weak as the one we found (figure 4.3a). This could be because the overturning is more dependent on the used forcing than we initially thought. It could be that the forcing we used was too idealised to find multiple equilibria.

The SSS and SST found in Baatsen et al. (2020) is also higher than the SSS and SST we found (figures 4.4c and 4.6a). They found a SST around the equator of around 35 °C, while with this model we found a SST of 26 °C. They found a SST for the southern polar of around 10 °C, which is much higher than the 0 °C we found. Tichelaar et al. (2011) found a SST at the equator of around 30 °C and a SST for the southern polar of around 15 °C, which are also higher than the SST's we found. The differences in SST could occur because different forcings were used. They could also occur because both Baatsen et al. (2020) and Tichelaar et al. (2011) used a coupled ocean-atmosphere model, and for this thesis we used an ocean model.

Deep water formation in Baatsen et al. (2020) occurs only in the Pacific sector of the Southern Ocean in winter. This is inconsistent with figure 4.5, which indicates that sinking takes place in the North Atlantic Ocean in our model. Even after the perturbation there is no pronounced deep water formation in the Pacific sector of the Southern Ocean. The location of the deep water formation is also illustrated in figure 4.3c. There is a southern sinking present at year 900, but it is very shallow. It can also be seen

in figure 4.1 that the time series of the MOC is not constant. This means that this shallow anti-clockwise overturning could still change into a clockwise overturning, with still deep water formation in the North Atlantic Ocean. The difference in the location of the deep water formation could occur because of the different forcing that was used.

Hutchinson et al. (2018) [26] use as initial conditions of the ocean model the following profile for the temperature and the salinity:

$$\begin{aligned} T(^\circ\text{C}) &= (500 - z)/5000 \cdot 20cos(\phi) + 10; \text{if z} \leq 5000\text{m} \\ &= 10; \text{if z} > 5000\text{m} \\ S(\text{psu}) &= 35.0, \end{aligned}$$

Where ϕ is the latitude and z is depth of the ocean. This is warmer and saltier than in the forcing used in this thesis. With this forcing, they find that the model exhibits sinking in the North Pacific and the Southern Ocean, which is contrary to figure 4.3a. Their SSS indicates very fresh conditions in the Arctic Ocean, around 20 g/kg. Around Greenland their SSS is still generally below 30 g/kg. In this thesis we found the lowest SSS (figure 4.4a) to also be in the be in the Arctic Ocean, but with a value of around around 32 g/kg. They find higher values for the SSS around the equator.
For the SST Hutchinson et al. (2018) find the equatorial SST to be as high as 38°C in the western Pacific, with tropical temperatures around 30–35°C elsewhere. The also find the high latitude SSTs of the North Pacific and Southern Ocean to be around 15–20°C, even along the coast of Antarctica. This is much warmer than the temperatures found in figure 4.6a.

Elsworth et al. (2017) [37] find that when the Drake Passage is closed or very shallow, Southern Ocean surface waters tend to be considerably denser than those of the North Atlantic. Consequently, deep water formation takes place in the Southern Ocean. They find that when the drake passage is open, the Southern Ocean surface freshens. The decrease in density of Southern Ocean surface waters provides an opportunity for North Atlantic waters to assume the role of deep water generation via the AMOC.

This all means that deep water formation in the Northern Atlantic can only take place when the Drake Passage is open. In this thesis the Drake passage is closed, so that means that the deep water formation in the Northern Atlantic should not have appeared.

From all this we can conclude that the used forcing is more important for the strength of the MOC than we initially thought. The MOC is highly sensitive to small changes in the surface forcing. Veros is a seasonally forced model. The forcing we used did not have seasonal fluctuations. There have been studies that suggest that these seasonal forcings can have a large effect on the strength of the MOC (Schmittner & Stocker, 2001) [38]. The idealised forcing that we used in this thesis could be the cause of the weaker MOC, the lower SSS and the lower SST than in Baatsen et al. (2020) and Hutchinson et al. (2018). It could also be the reason for the difference in location of deep water formation.

6 Conclusion

As can be seen in section 3.2, we did find an evident second equilibrium in the present-day geometry. The results found are also consistent with other studies on multiple equilibria in the present-day MOC. This means that Veros is indeed capable of finding multiple equilibria.

For the Eocene geometry we used the same procedure as described in section 2.2 and executed in section 3.2. We did find a different overturning pattern than in the Eocene reference state, but it was not in equilibrium. We also found that the SST did not change much before and after the perturbation. So if under these idealised forcing conditions two equilibria exist, they do not have a large influence on the heat distribution. This means that multiple equilibria with these forcing conditions would not contribute to Antarctic ice growth.

Instead of deep water formation in the Southern Ocean, we found only deep water formation in the Northern Atlantic Ocean in this model. The forcing we used in this thesis was too idealised to find multiple equilibria in Veros. Because Veros is a seasonally forced model, the idealised forcing that we used in this thesis failed to capture the seasonal changes, especially in the SST.

Because we did not find an evident second equilibrium in the Eocene geometry, there were no significant changes in the global heat distribution which you would get if there was a shift from a southern towards a northern overturning circulation. These changes would have made the Southern Hemisphere climate more susceptible for significant cooling and ice sheet formation on Antarctica.

For a next research, we should use a more realistic forcing, instead of the idealised one. For this, we could look at a coupled ocean-atmosphere model. We could, for example, use the same forcing used in Baatsen et al. (2020). They use a forcing that has a reduced equator-to-pole temperature gradient and a more symmetric meridional heat distribution compared to the present-day geometry. The forcing from a coupled ocean-atmosphere model generates the fields that we could use as a forcing in an ocean-only model. We would have to implement this forcing into Veros. Then we would have to run the model into a steady state. When it is in a steady state, we can see if we find the deep water formation in the Southern Ocean. We should also verify that we find the same SSS and SST as Baatsen et al. (2020). When this is the case, we can try to find the second equilibrium in the Eocene geometry with the same procedure we used for the present-day geometry in section 3.2.

There is currently no ice sheet model in Veros, but if that ever gets implemented, we could use it to model the total ice volume on Antarctica when we have found a second equilibrium. This way we could research the connection between a change in the MOC and land-ice growth in Antarctica.

References

[1] Baatsen, Michiel & Heydt, Anna S. & Huber, Matthew & Kliphuis, Michael & Bijl, Peter & Sluijs, Appy & Dijkstra, Henk. (2018). Equilibrium state and sensitivity of the simulated middle-to-late Eocene climate. Climate of the Past Discussions. 1-49. 10.5194/cp-2018-43.

[2] Tigchelaar, M & Heydt, Anna S. & Dijkstra, H. (2020). Climate of the Past A new mechanism for the two-step δ18 O signal at the Eocene-Oligocene boundary.

[3] Coxall, Helen & Wilson, Paul & Pälike, Heiko & Lear, Caroline & Backman, Jan. (2005). Rapid stepwise onset of Antarctic glaciation and deeper calcite compensation in the Pacific Ocean. Nature. 433. 53-7. 10.1038/nature03135.

[4] Coxall, Helen & Pearson, Paul. (2007). The Eocene-Oligocene Transition. Geological Society Special Publication. 2. 351-387.

[5] Thomas, DJ et al. (2003): Neodymium isotopic reconstruction of late Paleocene-early Eocene thermohaline circulation. Earth and Planetary Science Letters, 209(3-4), 309-322, https://doi.org/10.1016/S0012-821X(03)00096-7

[6] DeConto, R., Pollard, D. Rapid Cenozoic glaciation of Antarctica induced by declining atmospheric CO2. Nature 421, 245–249 (2003). https://doi.org/10.1038/nature01290

[7] Goldner, A. & Herold, Nicholas Huber, M.. (2014). The challenge of simulating the warmth of the mid-Miocene climatic optimum in CESM1. Climate of the Past. 10. 10.5194/cp-10-523-2014.

[8] Robert Toggweiler, Caitlin M. Amos, Ocean Circulation: Meridional Overturning Circulation, Editor(s): J. Kirk Cochran, Henry J. Bokuniewicz, Patricia L. Yager, Encyclopedia of Ocean Sciences (Third Edition), Academic Press, 2019, Pages 135-140, ISBN 9780128130827, https://doi.org/10.1016/B978-0-12-409548-9.11337-5.

[9] Schmittner, Andreas Chiang, John Hemming, Sidney. (2007). Introduction: The Ocean's Meridional Overturning Circulation. Geophys. Monogr. Ser.. 173. 10.1029/173GM02.

[10] Drijfhout, S.S. and W. Hazeleger, 2007. Detecting Atlantic MOC changes in an ensemble of climate change simulations. J. Climate, 20, Pages 1571-1582.

[11] Weijer, W., Cheng, W., Drijfhout, S. S., Federov, A.V., Hu, A., Jackson, L. C., et al. (2019). Stability of the Atlantic Meridional Overturning Circulation: A review and synthesis. Journal of Geophysical Research: Oceans, 124, 5336–5375. https://doi.org/10.1029/ 2019JC015083

[12] Rahmstorf, S. On the freshwater forcing and transport of the Atlantic thermohaline circulation. Climate Dynamics 12, 799–811 (1996). https://doi-org.proxy.library.uu.nl/10.1007/s003820050144

[13] Aken, Hendrik. (2007). The Oceanic Thermohaline Circulation: An Introduction, Pages 242-260.

[14] Stommel, H.: Thermohaline Convection with Two Stable Regimes of Flow, Tellus 13, Pages 224-230, 1961.

[15] Marotzke, J., 1990. Instabilities and Multiple Equilibria of the Thermohaline Circulation. Ph.D. Thesis, University of Kiel.

[16] Claes Rooth, Hydrology and ocean circulation, Progress in Oceanography, Volume 11, Issue 2, 1982, Pages 131-149, ISSN 0079-6611, https://doi.org/10.1016/0079-6611(82)90006-4.

[17] Scott, J. R., J. Marotzke, and P. H. Stone, 1999: Interhemispheric thermohaline circulation in a coupled box model. J. Phys. Oceanogr., 29, Pages 351–365.

[18] Dijkstra, Henk. (2005). Nonlinear Physical Oceanography: A Dynamical Systems Approach to the Large Scale Ocean Circulation and El Niño. Pages 71-74, 10.1007/1-4020-2263-8.

[19] Dijkstra, H. A., and Weijer, W.: Stability of the global ocean circulation: The connection of equilibria within a hierarchy of models, Journal of Marine Research, 61, 725-743, 2003.

[20] Olbers, Dirk & Zhang, Jian. (2008). The global thermohaline circulation in box and spectral low-order models. Part 1: Single basin models. Ocean Dynamics. 58. 311-334. 10.1007/s10236-008-0156-3.

[21] Jian Zhang (2007): Box and Low-order Models of the Thermohaline Circulation. MSC. Thesis, University of Bremen.

[22] Liu, Wei & Liu, Zhengyu. (2013). A Diagnostic Indicator of the Stability of the Atlantic Meridional Overturning Circulation in CCSM3. Journal of Climate. 26. 1926-1938. 10.1175/JCLI-D-11-00681.1.

[23] Steven M. Stanley, John A. Luczaj, Earth System History, New York, NY: W.H. Freeman and Company, a Macmillan Higher Education Company, Fourth edition (2015), Pages 449-475, ISBN 9781429255264.

[24] Gutjahr, Marcus; Ridgwell, Andy; Sexton, Philip F.; Anagnostou, Eleni; Pearson, Paul N.; Pälike, Heiko; Norris, Richard D.; Thomas, Ellen; Foster, Gavin L. (August 2017). "Very large release of mostly volcanic carbon during the Palaeocene–Eocene Thermal Maximum". Nature. 548 (7669): 573–577. doi:10.1038/nature23646

[25] Pearson, P. N.; Palmer, M. R. (2000). "Atmospheric carbon dioxide concentrations over the past 60 million years". Nature. 406 (6797): 695–699. doi:10.1038/35021000.

[26] Hutchinson, David & De Boer, Agatha & Coxall, Helen & Caballero, Rodrigo & Nilsson, Johan & Baatsen, Michiel. (2018). Climate sensitivity and meridional overturning circulation in the late Eocene using GFDL CM2.1. Climate of the Past Discussions. 1-46. 10.5194/cp-2017-161.

[27] Zhang, Yurui & Huck, Thierry & Lique, Camille & Donnadieu, Yannick & Ladant, Jean-Baptiste & Rabineau, Marina Daniel, Aslanian. (2020). Early Eocene vigorous ocean overturning and its contribution to a warm Southern Ocean. 10.5194/cp-2019-163.

[28] Häfner, Dion & Jacobsen, René & Eden, Carsten & Kristensen, Mads & Jochum, Markus & Nuterman, Roman & Vinter, Brian. (2018). Veros v0.1 – a Fast and Versatile Ocean Simulator in Pure Python. Geoscientific Model Development Discussions. 1-22. 10.5194/gmd-2018-3.

[29] Gebbie, J. and Huybers, P.: Meridional circulation during the Last Glacial Maximum explored through a combination of South Atlantic d18O observations and a geostrophic inverse model, Geochem. Geophy. Geosy., 7, 394–407, 2006.

[30] https://veros.readthedocs.io/en/latest/quickstart/introduction/

[31] Baatsen, Michiel Heydt, Anna S. Kliphuis, M. Viebahn, Jan Dijkstra, H.A.. (2018). Multiple states in the late Eocene ocean circulation. Global and Planetary Change. 163. 18-28. 10.1016/j.gloplacha.2018.02.009.

[32] Park, Young-Gyu. (1999). The Stability of Thermohaline Circulation in a Two-Box Model. Journal of Physical Oceanography - J PHYS OCEANOGR. 29. 3101-3110. 10.1175/1520-0485(1999).

[33] Marotzke, J., and J. Willebrand. 1991. Multiple Equilibria of the Global Thermohaline Circulation. Journal of Physical Oceanography 21:1372-1385.

[34] Dijkstra, H. A., 2008: Scaling of the Atlantic meridional overturning in a global ocean model. Tellus, 60A, 749–760, doi:10.1111/j.1600-0870.2008.00326.x.

[35] Huisman, Selma & Toom, Matthijs & Dijkstra, Henk & Drijfhout, Sybren. (2010). An Indicator of the Multiple Equilibria Regime of the Atlantic Meridional Overturning Circulation. J. Phys. Oceanogr.. 40. 10.1175/2009JPO4215.1.

[36] Baatsen, M., von der Heydt, A. S., Huber, M., Kliphuis, M. A., Bijl, P. K., Sluijs, A., and Dijkstra, H. A.: The middle-to-late Eocene greenhouse climate, modelled using the CESM 1.0.5, Clim. Past Discuss., https://doi.org/10.5194/cp-2020-29,inreview,2020.

[37] Elsworth, G., Galbraith, E., Halverson, G. et al. Enhanced weathering and CO2 drawdown caused by latest Eocene strengthening of the Atlantic meridional overturning circulation. Nature Geosci 10, 213–216 (2017). https://doi.org/10.1038/ngeo2888

[38] Schmittner, A., and T. F. Stocker, A seasonally forced ocean-atmosphere model for paleoclimate studies, J. Clim., 14, 1055–1068, 2001.

A Appendix

A.1 Idealised Forcing Conditions

The used idealised forcing profiles are made by Marte Voorneveld for his Bachelor Thesis. The forcing profiles for the SSS and SST for the Eocene are shown in figure A.1 and figure A.2. The forcing profiles are symmetrical in the meridional direction. Figure A.3 shows the wind forcing in the zonal direction. This profile is also symmetrical in the meridional direction. The wind forcing in the meridional direction is zero everywhere in this setup. The used contour plots of the salinity and temperature are shown in figure A.4 and figure A.5. They are the same for every degree longitude.

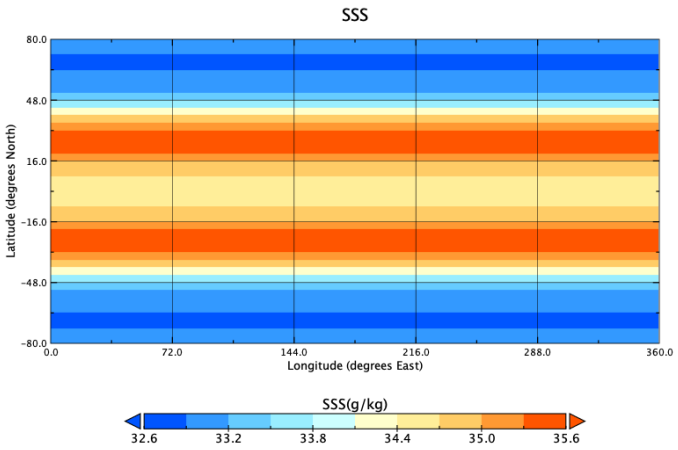

Figure A.1: The forcing profile for the SSS.

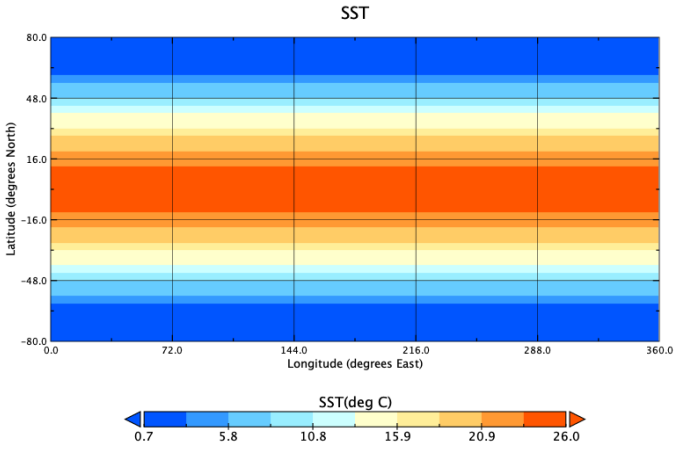

Figure A.2: The forcing profile for the SST.

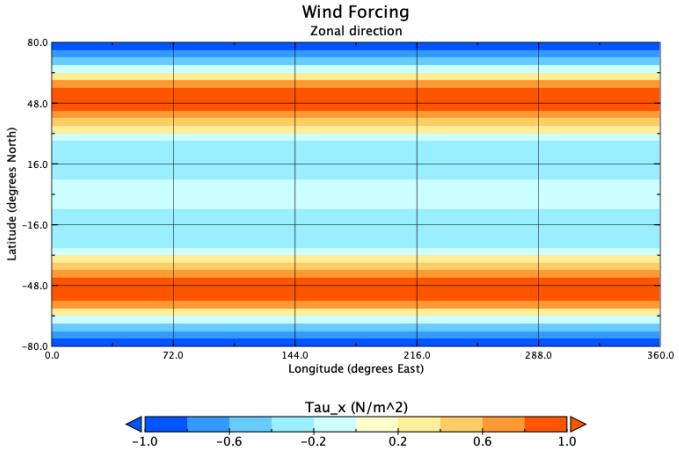

Figure A.3: The forcing profile for the wind in the zonal direction.

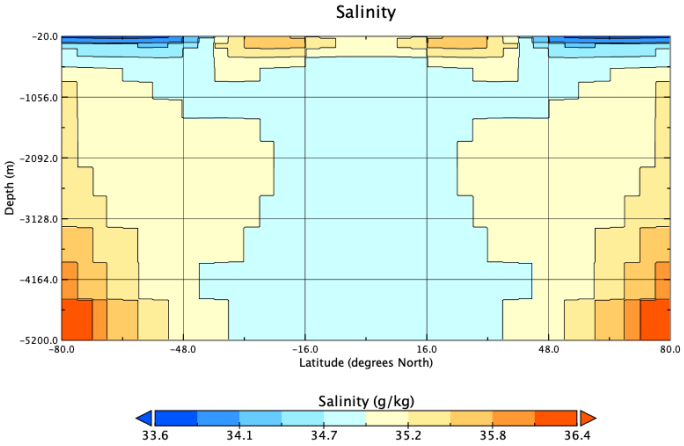

Figure A.4: A contour plot of the salinity of the idealised forcing. The forcing is the same for every degree longitude.

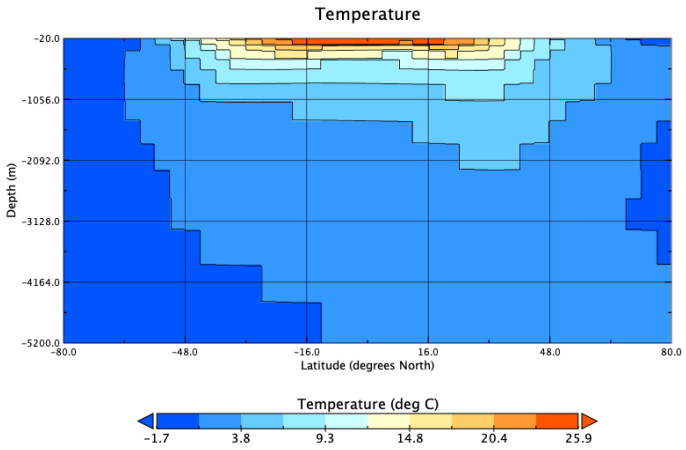

Figure A.5: A contour plot of the temperature of the idealised forcing. The forcing is the same for every degree longitude.

A.2 GitHub

The adapted Veros codes for the present-day and the Eocene geometry can be found on GitHub, as well as the used bathymetry and idealised forcing conditions of the Eocene geometry. The scripts for the figures can also be found there.
Link: `https://github.com/deniseruijsch/Multiple-equilibria-in-the-Eocene-ocean-circulation-leading-to-the-Eocene-Oligocene-transition.git`